
Chapter 1 Composition of Accelerator Radiation Fields

In this chapter, terminology, physical and radiological quantities, and units of measurement used to describe the properties of accelerator radiation fields are reviewed. The general considerations of primary radiation fields pertinent to particle accelerators are discussed both qualitatively and quantitatively.

I. Review of Units, Terminology, Physical Constants, and Material Properties

Radiological Units

We must begin our discussion by introducing some units of measure and terminology commonly used in accelerator radiation protection.

energy: The unit of energy in common use when dealing with energetic particles is the electron volt (eV) $1 \text{ eV} = 1.602 \times 10^{-12} \text{ ergs}$ or $1.602 \times 10^{-19} \text{ Joule}$. Multiples in common use at accelerators are the keV (10^3 eV), MeV (10^6 eV), GeV (10^9 eV), and TeV (10^{12} eV).

absorbed dose: The energy absorbed per unit mass of material. It is usually denoted by the symbol D . The customary unit of absorbed dose is the **rad** while the *Système Internationale* (SI) unit of absorbed dose is the **Gray**:

$$\begin{aligned} 1 \text{ rad} &= 100 \text{ ergs/gram} = 6.24 \times 10^{13} \text{ eV/gm} \\ 1 \text{ Gray (Gy)} &= 1 \text{ J/kg} = 100 \text{ rads} = 6.24 \times 10^{15} \text{ eV/gm.} \end{aligned}$$

dose equivalent: This quantity has the same dimensions as absorbed dose. It is used to take into account the fact that different particle types have biological effects which are enhanced, per given absorbed dose, over those due to 200 keV photons (a "standard" reference particle). It is usually denoted by the symbol H . The customary unit is the **rem** while the SI unit is the **Sievert** (Sv).

quality factor: This factor takes into account the relative enhancement in biological effects of various types of ionizing radiation. It is usually denoted by Q , and is used to obtain H from D through the following equation:

$$H = QD. \quad (1.1)$$

Q is dependent on both particle type and energy and, thus, for any radiation field its value is an average over all components. It is defined to be equal to unity for 200 keV photons. Q ranges from unity for photons electrons, and high energy muons to a value as large as 20 for α -particles (^4He nuclei) of a few MeV in energy. For neutrons, Q ranges from 2 to greater than 10, although recent guidance by the International Council on Radiation Protection (ICRP) has recommended increased values of Q for neutrons (IC91). The latter guidance has yet to be adopted by United States regulatory authorities.

Chapter 1 Composition of Accelerator Radiation Fields

Q is presently defined to be a function of **linear energy transfer** (LET), L , which, crudely, is equivalent to **stopping power**, or rate of energy loss for charged particles and is conventionally expressed in units of keV/micron. All ionizing radiation ultimately manifests itself through charged particles so that LET is a "universal" measure of localized radiation damage.

The value of Q commonly used is an average over the spectrum of LET present:

$$\langle Q \rangle = \frac{\int_0^{\infty} Q(L)D(L)dL}{\int_0^{\infty} D(L)dL}. \quad (1.2)$$

Thus, H (rem) = $Q D$ (rads) or H (Sv) = QD (Gy). Figures 1.1, 1.2, and 1.3 give the relationships between Q and LET and Q as a function of particle energy for a variety of particles.

flux density-The number of particles that traverse a unit area in unit time, generally denoted by the symbol ϕ ,

$$\phi = \frac{d^2n}{dA dt} \quad (1.3)$$

where d^2n is the differential number of particles traversing surface area element dA during time dt . For radiation fields where the constituent particles move in a multitude of directions, ϕ is determined from the number of transversals of a sphere of revolution of a small element of circular area dA . The units of flux density are $\text{cm}^{-2}\text{s}^{-1}$ (customary) and $\text{m}^{-2}\text{s}^{-1}$ (SI).

fluence, denoted by Φ , is simply the time integral over some time interval of the flux density,

$$\Phi = \int_{t_i}^{t_f} \phi(t) dt. \quad (1.4)$$

The units of fluence are, of course, inverse area. The reader is cautioned that other units of time such as hours, minutes, days, years, etc. are commonly seen in the literature.

dose equivalent per unit fluence conversion factors - Such factors have been derived theoretically and supported in a limited way by measurements. They include effects due to the finite thicknesses of the material of reference (usually "tissue") and include secondary effects. Figures 1.4 and 1.5 are adapted from the tabulations of Schopper et al. (Sc90).

Chapter 1 Composition of Accelerator Radiation Fields

For a radiation field containing a mixture of n different components (c.g., different particle types), one determines the dose equivalent, H , from:

$$H = \sum_{i=1}^n \int_{E_{\min}}^{E_{\max}} P_i(E) \Phi_i(E) dE \quad (1.5)$$

where $\Phi_i(E)$ is the fluence of particles of type i with energy between E and dE and $P_i(E)$ is the dose equivalent per unit fluence in appropriate units.

The **cross section** is an extremely important physical concept in describing particle interactions. The cross section represents the "size" of the atom or nucleus for some particular interaction. Consider a beam of particles of fluence Φ (particles/cm²) incident on a thin slab of absorber of thickness dx . The absorbing medium contains N atoms/cm³. The number of incident particles which interact and are "lost" from the original fluence, $-d\Phi$, is given by:

$$-d\Phi = \sigma N \Phi dx \quad (1.6)$$

where σ is the cross section (cm²). But, $N = \rho N_A / A$, where ρ is the density (g/cm³), N_A is Avogadro's number (6.02×10^{23} mol⁻¹) and A is the atomic weight. Cross sections are often given in units of **barns** where 1 barn = 10^{-24} cm². If only one physical process is present with no others are operative and if one starts with an initial fluence Φ_0 , this integrates, after some distance x (cm), to:

$$\Phi(x) = \Phi_0 e^{-N\sigma x} \quad (1.7)$$

The **linear absorption coefficient**, μ , and its reciprocal, the **attenuation length**, λ , are given by:

$$\mu = N\sigma \text{ (cm}^{-1}\text{)} \quad \lambda = 1/N\sigma \text{ (cm)}. \quad (1.8)$$

Sometimes the mass attenuation length, $\lambda_m = \rho/N\sigma$ (g/cm²), is used where ρ is the density in g/cm³. Unfortunately, in the literature, λ is often used for λ_m so that one has to take care to understand the context to be sure to use the correct units. For high energy particles subject to the **strong, or nuclear interaction**, λ is commonly called the **interaction length**.

Physical Constants and Atomic and Nuclear Properties

Tables 1.1 and 1.2 give physical constants and atomic and nuclear properties as tabulated by the Particle Data Group (PDG96). A number of these constants and properties will be used throughout the rest of this text and in the solutions of the problems.

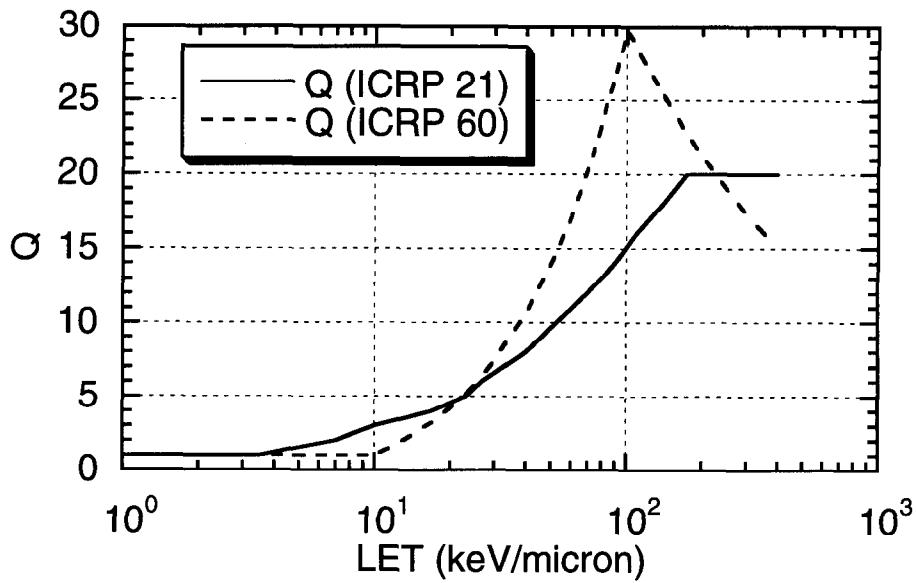


Fig. 1.1 Quality Factor, Q , of charged particles as a function of collision stopping power (LET) in water as recommended by ICRP Reports 21 (IC73) and 60 (IC91).

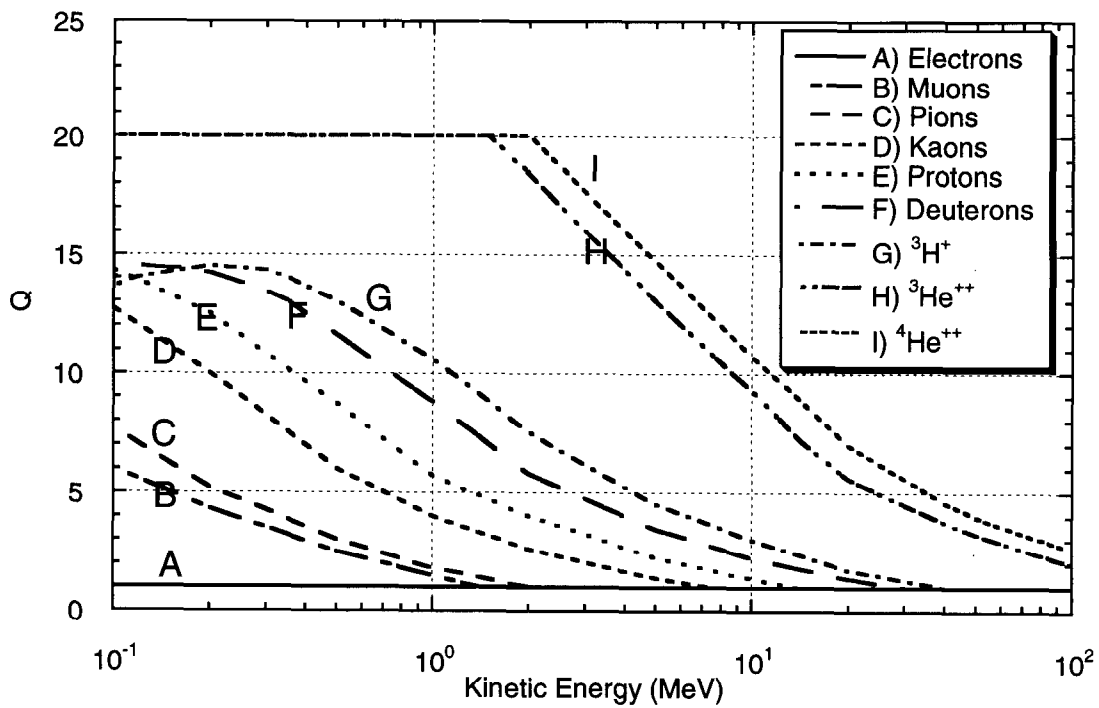


Fig. 1.2 Quality factors of charged particles as a function of energy, as recommended by the ICRP. [Adapted from (Pa73) and (IC73)].

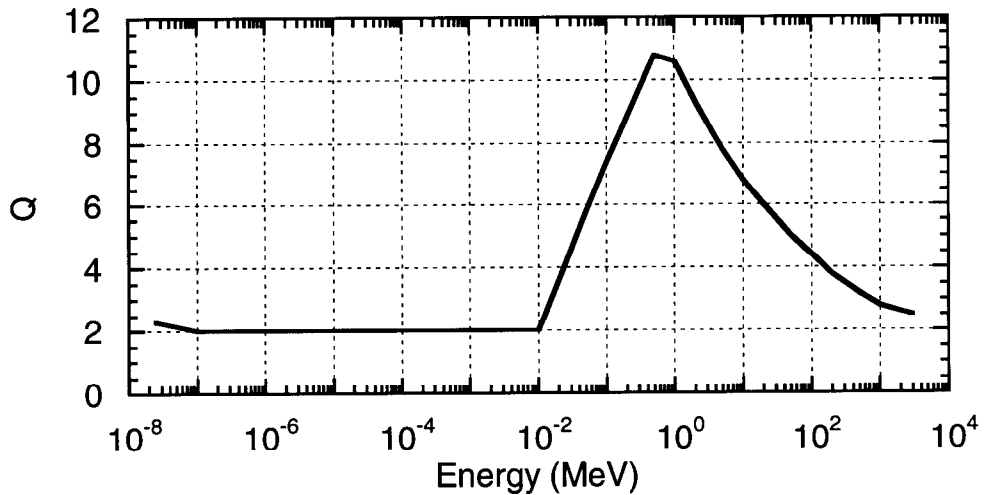


Fig. 1.3 Effective quality factor, Q , for neutrons as a function of neutron kinetic energy: the maximum dose equivalent divided by the absorbed dose where the maximum dose equivalent occurs (IC73) in human tissue. [Adapted from (Pa73).]

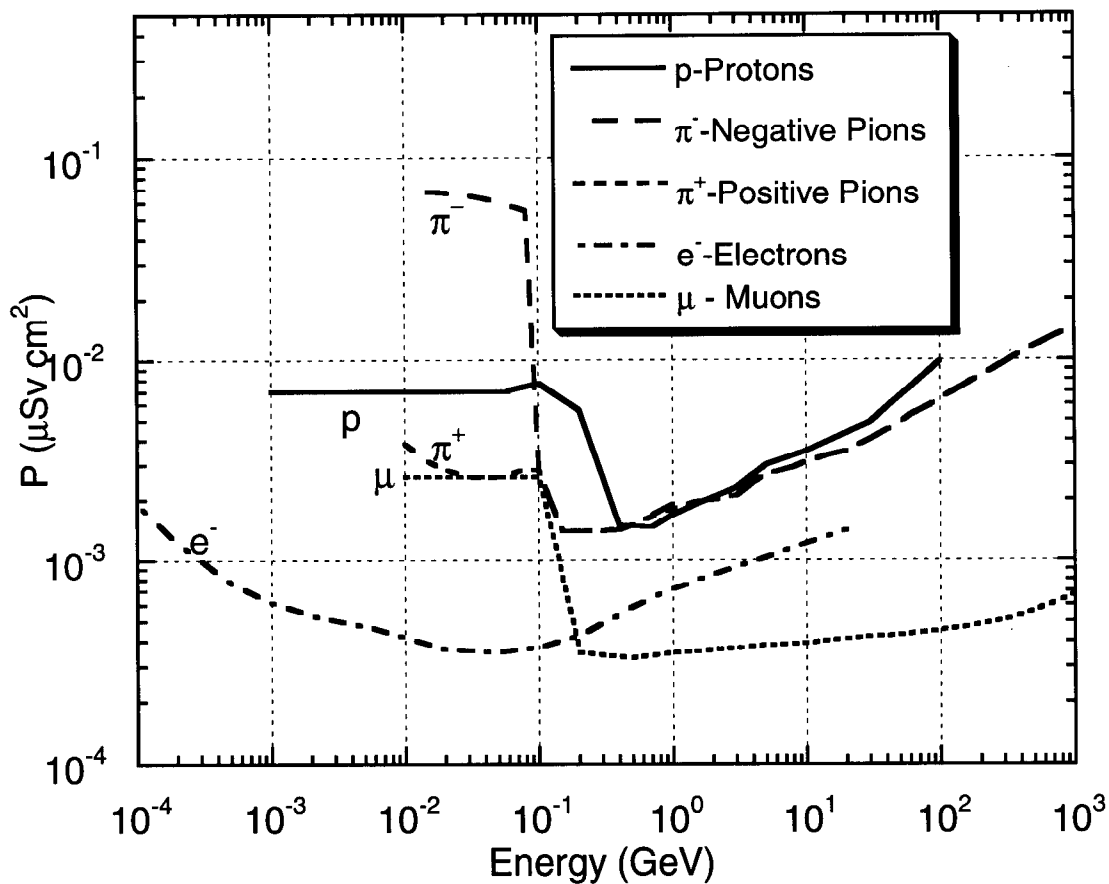


Fig. 1.4 Dose equivalent per unit fluence for various charged particles, P , as a function of energy. The curve for muons is valid for both negative and positively-charged muons. [Adapted from (Sc90).]

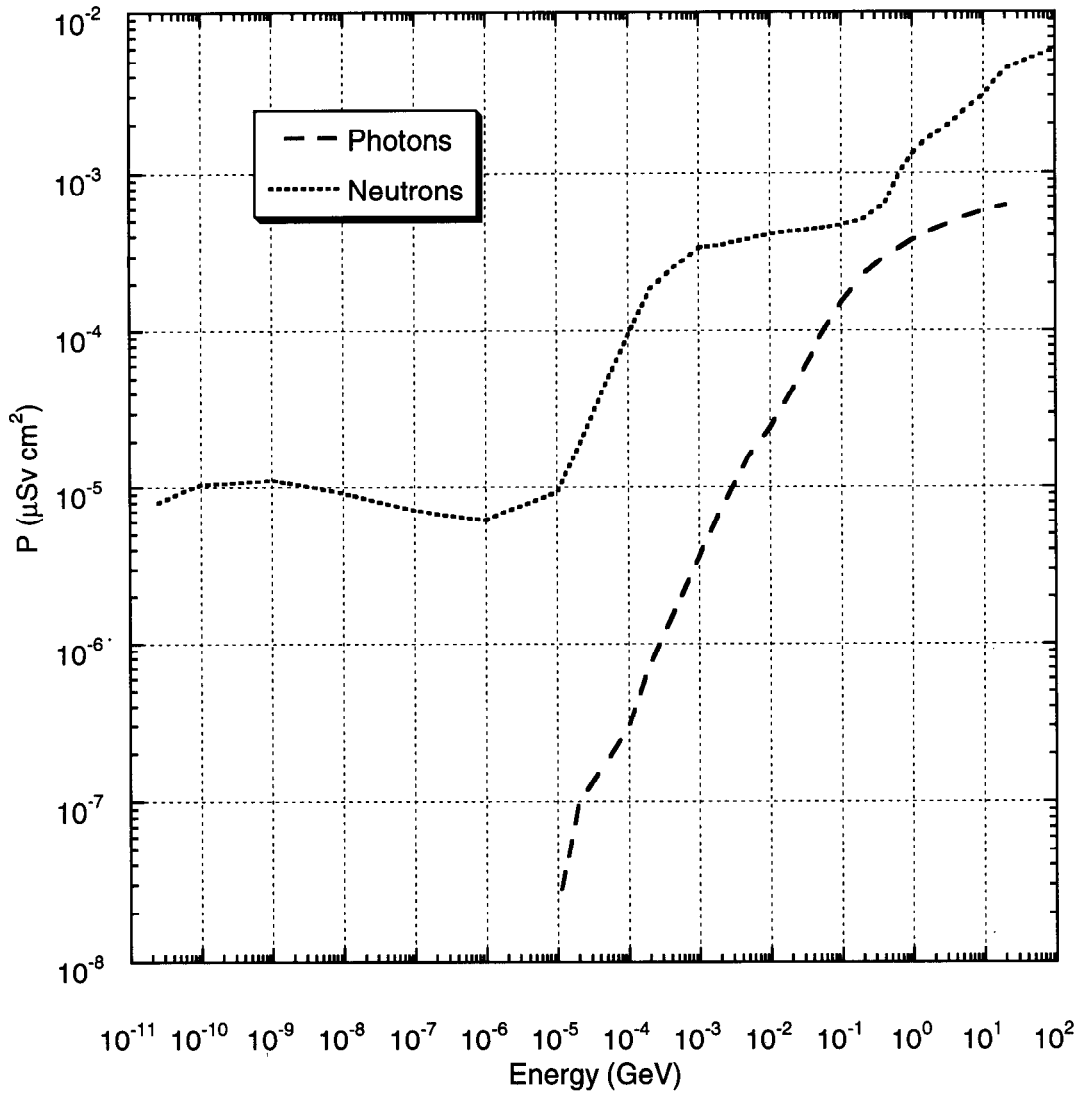


Fig. 1.5 Dose equivalent per unit fluence for photons and neutrons, P , as a function of energy. [Adapted from (Sc90).]

Chapter 1 Composition of Accelerator Radiation Fields

Table 1.1 Physical constants [Adapted from (PDG96)]

Quantity	Symbol, Equation	Value ^a
speed of light	c	$2.99792458 \times 10^8 \text{ m s}^{-1}$
Planck constant	h	$6.6260755(40) \times 10^{-34} \text{ J s}$
Planck constant, reduced	$\hbar = h/2\pi$	$1.05457266(63) \times 10^{-34} \text{ J s}$ $= 6.5821220(20) \times 10^{-22} \text{ MeV s}$
electron charge	e	$1.60217733(49) \times 10^{-19} \text{ C}$
useful constant	$\hbar c$	$197.327053(59) \text{ MeV fm}$
useful constant	$(\hbar c)^2$	$0.38937966(23) \text{ GeV}^2 \text{ mbarn}$
electron mass	m_e	$0.51099906(15) \text{ MeV}/c^2$ $= 9.1093897(54) \times 10^{-31} \text{ kg}$
proton mass	m_p	$938.27231(28) \text{ MeV}/c^2$ $= 1.6726231(10) \times 10^{-27} \text{ kg}$ $= 1.007276470(12) \text{ u}$ $= 1836.152701(37) m_e$
deuteron mass	m_d	$1875.61339(57) \text{ MeV}/c^2$
unified atomic mass unit (u)	$(\text{mass } ^{12}\text{C atom})/12$ $= (1 \text{ g})/N_A$	$931.49432(28) \text{ MeV}/c^2$ $= 1.6605402(10) \times 10^{-27} \text{ kg}$
permittivity of free space	ϵ_0	$8.854187817 \times 10^{-12} \text{ F m}^{-1}$
permeability of free space	μ_0 $[\epsilon_0 \mu_0 = 1/c^2]$	$4\pi \times 10^{-7} \text{ N A}^{-2}$
fine structure constant	$\alpha = e^2/4\pi \epsilon_0 \hbar c$	$1/137.0359895(61)$
classical electron radius	$r_e = e^2/4\pi \epsilon_0 m_e c^2$	$2.81794092(38) \times 10^{-15} \text{ m}$
electron compton wavelength	$\lambda_e = \hbar/m_e c$	$3.86159323(35) \times 10^{-13} \text{ m}$
wavelength of 1 eV/c particle	hc/e	$1.23984244(37) \times 10^{-6} \text{ m}$
Thomson cross section	$\sigma_T = 8\pi r_e^2/e$	$0.66524616(18) \text{ barn}$
gravitational constant	G_N	$6.67259(85) \times 10^{-11} \text{ m}^3 \text{ kg}^{-1} \text{ s}^{-2}$
std. gravitational accel.	g	9.80665 m s^{-2}
Avogadro number	N_A	$6.0221367(36) \times 10^{23} \text{ mol}^{-1}$
Boltzmann constant	k	$1.380658(12) \times 10^{-23} \text{ J K}^{-1}$
	1 barn	10^{-28} m^2
	1 eV	$1.60217733(49) \times 10^{-19} \text{ J}$
	1 Gauss	10^{-4} Tesla
	1 erg	10^{-7} J
	1 fm	10^{-15} m
	1 atmosphere	$760 \text{ torr} = 1.01325 \times 10^5 \text{ N/m}^2$
	0° C	$273.15 \text{ }^\circ\text{K}$

^a The one-standard deviation uncertainties in the last digits are given in parentheses.

Chapter 1 Composition of Accelerator Radiation Fields

Table 1.2 Atomic and nuclear properties of materials [Adapted from (PDG96)]

Mat'l	Z	A	Nu- clear total cross sect. ^a σ_T (barn)	Nucle- ar inelas- tic cross sect. ^a σ_{in} (barn)	Nucle- ar col- lision length ^b λ_T (g/cm ²)	Nucle- ar inter- action length ^b λ_{in} (g/cm ²)	Min. stop- ping power ^c dE/dx (MeV/ g/cm ²)	Radia- tion X_o (g/cm ²)	Length X_o (cm) () is for gas	Density ^d ρ (g/cm ³) () or [] for gas (g/l)
H ₂	1	1.01	0.0387	0.033	43.3	50.8	4.12	61.28	865	0.0708(0.090)
D ₂	1	2.01	0.073	0.061	45.7	54.7	2.07	122.6	757	0.162[0.179]
He	2	4.00	0.133	0.102	49.9	65.1	1.94	94.32	755	0.125[0.179]
Li	3	6.94	0.211	0.157	54.6	73.4	1.58	82.76	155	0.534
Be	4	9.01	0.268	0.199	55.8	75.2	1.61	65.19	35.3	1.848
C	6	12.01	0.331	0.231	60.2	86.3	1.78	42.70	18.8	2.265 ^e
N ₂	7	14.01	0.379	0.265	61.4	87.8	1.82	37.99	47.0	0.808[1.25]
O ₂	8	16.00	0.420	0.292	63.2	91.0	1.82	34.24	30.0	1.14[1.43]
Al	13	26.98	0.634	0.421	70.6	106.4	1.62	24.01	8.9	2.70
Si	14	28.09	0.660	0.440	70.6	106.0	1.66	21.82	9.36	2.33
Ar	18	39.95	0.868	0.566	76.4	117.2	1.51	19.55	14.0	1.40[1.78]
Fe	26	55.85	1.120	0.703	82.8	131.9	1.48	13.84	1.76	7.87
Cu	29	63.55	1.232	0.782	85.6	134.9	1.44	12.86	1.43	8.96
Ge	32	72.59	1.365	0.858	88.3	140.5	1.40	12.25	2.30	5.323
W	74	183.85	2.767	1.65	110.3	185	1.16	6.76	0.35	19.3
Pb	82	207.19	2.960	1.77	116.2	194	1.13	6.37	0.56	11.35
U	92	238.03	3.378	1.98	117.0	199	1.09	6.00	0.32	18.95
Air					62.0	90.0	1.82	36.66	(30420)	(1.205)[1.293]
H ₂ O					60.1	84.9	2.03	36.08	36.1	1.00
Shielding concrete ^f					67.4	99.9	1.70	26.7	10.7	2.5
SiO ₂ (quartz)					67.0	99.2	1.72	27.05	12.3	2.64
NaI					94.8	152	1.32	9.49	2.59	3.67
Polystyrene, scintillator (CH)					58.4	83.0	1.95	43.8	42.4	1.032
Polyethylene (CH ₂)					56.9	78.8	2.09	44.8	47.9	0.92-0.95
Mylar (C ₅ H ₄ O ₂)					60.2	85.7	1.86	39.95	28.7	1.39
CO ₂					62.4	90.5	1.82	36.2	(18321)	[1.977]
Methane (CH ₄)					54.7	74.0	2.41	46.5	(64850)	0.424[0.717]
Ethane (C ₂ H ₆)					55.7	75.7	2.30	45.7	(34035)	0.509(1.356)
NaF					66.78	97.57	1.69	29.87	11.68	2.558
LiF					62.0	88.24	1.66	39.25	14.91	2.632

^aThese are energy dependent. The values quoted are for the high energy limit. The inelastic cross section is obtained by subtracting the elastic and quasi-elastic cross sections from the total cross section.

^bThese quantities are the mean free path between all collisions (λ_T) or inelastic interactions (λ_{in}) and are also energy-dependent. The values quoted are for the high energy limit.

^cThis is the minimum value of the ionization stopping power for heavy particles. It is calculated for pions and the results are slightly different for other particles.

^dFor substances that are gases at room temperature, values at 20 °C and 1 atmosphere pressure are given in parentheses (grams/liter) while values at STP are given in square brackets [grams/liter]. Values without () or [] are for cryogenic liquids at the boiling point at 1 atmosphere pressure.

^eThe tabulated values are for pure graphite; industrial graphite may vary between 2.1-2.3 g cm⁻³.

^fThis is for standard shielding blocks, typical composition of O₂ (52%), Si (32.5%), Ca (6%), Na (1.5%), Fe (2%), Al (4%), plus reinforcing iron bars.

II. Summary of Relativistic Relationships

The **rest energy**, W_0 , of a particle of rest mass m_0 is given by,

$$W_0 = m_0 c^2, \quad (1.9)$$

where c is the velocity of light.

The **total energy** in free space, W , is then given by

$$W = mc^2 = m_0 c^2 (1 - \beta^2)^{-1/2}, \quad (1.10)$$

where $\beta = v/c$ and v is the velocity of the particle in a given frame of reference.

The **relativistic mass**, m , of a particle moving at β is another name for the total energy and is given by

$$mc^2 = \frac{1}{\sqrt{1 - \beta^2}} m_0 c^2 = \gamma m_0 c^2 \quad (1.11)$$

The **kinetic energy**, E , is then;

$$E = W - W_0 = (m - m_0)c^2 \quad \text{and} \quad (1.12)$$

$$\beta = \sqrt{1 - \left(\frac{W_0}{W}\right)^2}. \quad (1.13)$$

The **momentum**, p , of a particle is

$$p = mv = m\beta c = \frac{1}{c} \sqrt{E(E + 2W_0)} = \frac{1}{c} \sqrt{E(E + 2W_0)}, \quad (1.14)$$

so that at high energies, $p \approx E/c \approx W/c$.

It is usually most convenient to work in a system of units where energy is in units of eV, MeV, etc. Velocities are, then, expressed in units of the speed of light (β), momenta are expressed as energy divided by c (e.g., MeV/c, etc.), and masses are expressed as energy divided by c^2 (e.g., MeV/c², etc.).

For moderately relativistic particles, the mean rate of energy loss (**stopping power**) is given approximately by (PDG96):

$$-\frac{dE}{dx} = 4\pi N_A r_e^2 m_e c^2 z^2 \frac{Z}{A} \frac{1}{\beta^2} \left[\ln \left\{ \frac{2m_e c^2 \gamma^2 \beta^2}{I} \right\} - \beta^2 - \frac{\delta}{2} \right], \quad (1.15)$$

where N_A is Avogadro's number, Z and A are the atomic number and weight of the material transversed, z is the charge state of the projectile in units of electron charge, m_e and r_e are the mass and "classical radius" of the electron and I is the ionization constant. δ is a small correction factor which approaches $2 \ln \gamma$. Substituting constants,

$$-\frac{dE}{dx} = 0.3071z^2 \frac{Z}{A} \frac{1}{\beta^2} \left[\ln \left\{ \frac{2m_e c^2 \gamma^2 \beta^2}{I} \right\} - \beta^2 - \frac{\delta}{2} \right] \quad (\text{MeV cm}^2\text{g}^{-1}) \quad (1.16)$$

where $I \approx 16Z^{0.9}$ eV for $Z > 1$. I has a value of approximately 20 eV for diatomic hydrogen.

The **decay length** at a given velocity of a particle with a finite meanlife (at rest), τ , can be obtained from the product of the speed of light and the meanlife, $c\tau$, which is often tabulated. The decay length is given by $\beta c \gamma \tau$, where relativistic time dilation is taken into account by inclusion of the factor γ . This length is to be distinguished from that called the **decay path**. The latter represents a distance in space in which a given particle is allowed to decay with no or minimal competition from other effects such as by scattering or absorption.

III. Primary Radiation Fields at Accelerators-General Considerations

The particle **yield**, Y , is a crucial parameter. It is typically a function of both angle and particle energy and is defined according to Fig. 1.6. Such particle yields, dependent upon both target material and thickness, are reported in terms of particle type, energy, and angular distributions. Scattered reaction products are found at a "point of interest" located at radius, r , and polar angle, θ , relative to the direction of the incident particle along the positive Z -axis. The rate of production of the desired reaction products and their energy spectra is, in general, a strong function of both θ and the incident particle energy E_0 . There is usually no dependence on the azimuthal angle in a spherical coordinate system.¹

In principle, calculations of the particle yield could be taken directly from differential cross sections for given incident particle kinetic energy E ,

$$\frac{d\sigma(\theta, E)}{d\Omega},$$

where $\sigma(\theta, E)$ is the cross section as a function of energy and angle and Ω is the solid angle into which the secondary particles are produced. This would involve an integral of this cross section it varies while the incident particle passes through the target material. Calculations of the radiation field which directly use the cross sections are often not practical because targets hit by beam are not really thin (i.e., one cannot ignore energy loss or secondary interactions in the target). The knowledge of cross sections at all energies is generally incomplete with the unfortunate result that one commonly cannot integrate over θ and E to get the total yield.

¹The single exception is the case in which the spins of the target nuclei and/or the incident particle are oriented along some chosen direction in a "polarization" experiment.

Chapter 1 Composition of Accelerator Radiation Fields

For many applications, the details of the angular distributions of **total secondary particle yield**, $dY(\theta)/d\Omega$, and the **angular dependence of the emitted particle energy spectrum**, $d^2Y(\theta,E)/dEd\Omega$, of the emitted particle spectra are very important. Often, the particle fluence is needed at a particular location at coordinates (r, θ) from a known point source of beam loss while the angular distributions of $dY/d\Omega$ are generally expressed in units of particles/(steradian-incident particle).

To obtain the total fluence $\Phi(\theta)$ [e.g., particles/(cm²·incident particle)], or differential fluence $d\Phi(E, \theta)/dE$ [e.g., particles/(cm²·MeV·incident particle)] at a given distance r (cm) at a specified angle θ from such a **point source**, one must simply multiply the yield values by r^{-2} (cm⁻²):

$$\Phi(\theta) = \frac{1}{r^2} \frac{dY(\theta)}{d\Omega} \quad \text{and} \quad \frac{d\Phi(E, \theta)}{dE} = \frac{1}{r^2} \frac{d^2Y(\theta, E)}{dEd\Omega} \quad (1.17)$$

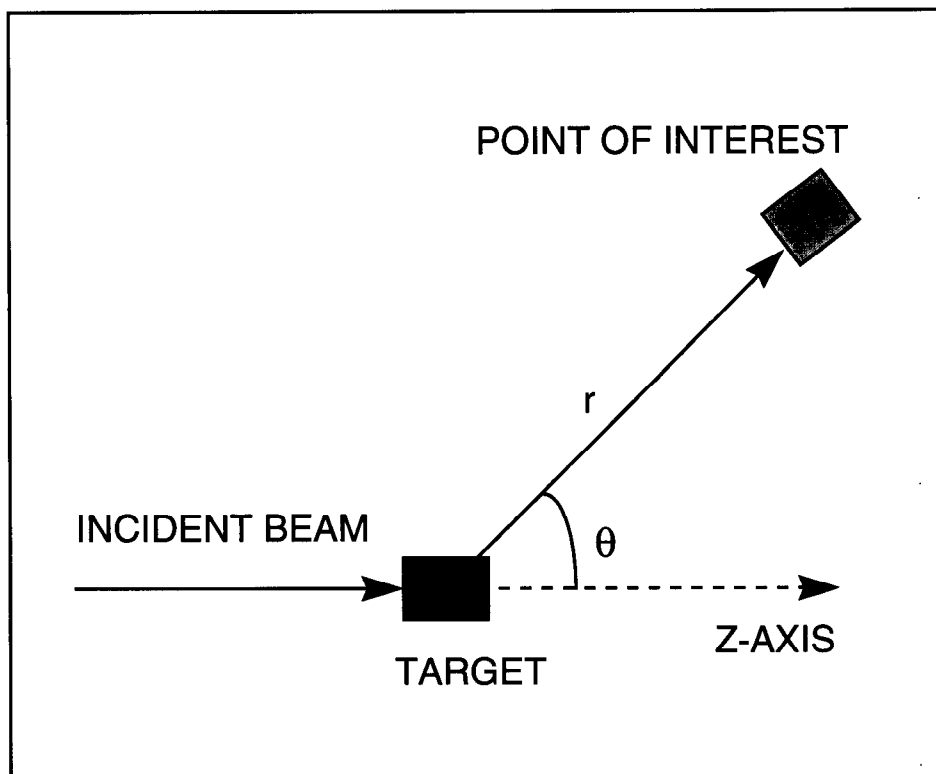


Fig. 1.6 Conceptual interaction of incident beam with material (target) which produces radiation at the point of interest located at polar coordinates (r, θ) .

IV. Radiation Production by Electron Accelerators

At all energies photons produced by **bremsstrahlung** dominate the radiation field aside from the hazard of the direct beam. As the energy increases, neutrons become a significant problem. For $E_o > 100$ MeV, the **electromagnetic cascade** must be considered (see Chapter 2). An interesting rule of thumb is that electrons have a finite range in any material proportional to the initial kinetic energy of the electron, E_o (MeV):

For $2 < E_o < 10$ MeV,

$$R = 0.6E_o \text{ g cm}^{-2}. \quad (1.18)$$

In air, R (meters) $\approx 5 E_o$ (MeV). Above approximately 10 MeV, **radiative** losses begin to dominate, as will be discussed shortly.

Direct Beam

Swanson (Sw79) has given a "conservative" rule of thumb for the electrons in the energy domain of $1 < E_o < 100$ MeV:

$$\frac{dH}{dt} = 1.6 \times 10^{-4} \phi, \quad (1.19)$$

where dH/dt is the dose equivalent rate (rem h⁻¹) and ϕ is the flux density (cm⁻² s⁻¹).

Bremsstrahlung

Bremsstrahlung is the radiative energy loss of electrons as they interact with materials. It appears in the form of photons. An important parameter when considering radiative energy loss of electrons in matter is the **critical energy**, E_c . The critical energy is the energy above which the energy loss due to radiation exceeds that due to ionization for electrons. The value of E_c is a smooth function of atomic number;

$$E_c = 800/(Z + 1.2) \text{ (MeV)}, \quad (1.20)$$

where Z is the atomic number of the material.

The transition from ionization to radiation is also a smooth one. The stopping power for electrons may be written as the sum of collisional and radiative components:

$$\left(\frac{dE}{dx}\right)_{tot} = \left(\frac{dE}{dx}\right)_{coll} + \left(\frac{dE}{dx}\right)_{rad} \quad (1.21)$$

A parameter of significant importance for electrons is the **radiation length**, X_o , which is the mean thickness of material over which a high energy electron loses all but $1/e$ of its

Chapter 1 Composition of Accelerator Radiation Fields

energy by bremsstrahlung and is the approximate scale length for describing high-energy electromagnetic cascades. This parameter also plays a role in the "scaling" of multiple scattering for all charged particles. It is approximated by:

$$X_0 = \frac{716.4A}{Z(Z+1)\ln(287/\sqrt{Z})} \quad (\text{g cm}^{-2}) \quad (1.22)$$

where Z and A are the atomic number and weight of the material medium, respectively. It turns out for high energy electrons that the rate of energy loss is given by:

$$\left(\frac{dE}{dx}\right)_{rad} = -\frac{E}{X_0}, \quad (1.23)$$

so that under these conditions (i.e., where ionization can be neglected), the energy, E , of the electron as a function of thickness of shield penetrated, x , is given by

$$E(x) = E_0 e^{-x/X_0} \quad (1.24)$$

where the energy of the incident particle is E_0 .

Figure 1.7 gives the percentage of energy E_0 that appears as radiation for various materials as a function of energy. External bremsstrahlung develops as a function of target thickness and is described by a "transition" curve. As the thickness increases, the radiation increases until reabsorption begins to take effect. Then, self-shielding begins to take over. One talks about the maximum as a "thick-target" bremsstrahlung spectrum. This phenomenon becomes important above energies of about 100 MeV for low- Z materials and above 10 MeV for high- Z materials. The energy spectrum of the radiated photons ranges from zero to the energy of the incident electron and the number of photons in a given energy interval is approximately inversely proportional to the photon energy. The amount of energy radiated per energy interval is practically constant according to Schopper et al. (Sc90). To address radiological concerns in a conservative manner, one often assumes the target to be "thick" in this sense. Figure 1.8 shows the behavior for a high- Z target. Swanson has developed three "rules of thumb" which parameterize this behavior for the absorbed dose rates, dD/dt , at one meter normalized to one kW of incident beam power for E_0 in MeV (Sw79):

Rule of Thumb 1:

$$\frac{dD}{dt} \approx 20E_0^2 \quad (\text{Gy h}^{-1})(\text{kW}^{-1} \text{ m}^2) \quad \text{at } \theta = 0^\circ, E_0 < 15 \text{ MeV}. \quad (1.25)$$

Rule of Thumb 2:

$$\frac{dD}{dt} \approx 300E_0 \quad (\text{Gy h}^{-1})(\text{kW}^{-1} \text{ m}^2) \quad \text{at } \theta = 0^\circ, E_0 > 15 \text{ MeV}. \quad (1.26)$$

Rule of Thumb 3:

$$\frac{dD}{dt} \approx 50 \quad (\text{Gy h}^{-1})(\text{kW}^{-1} \text{ m}^2) \quad \text{at } \theta = 90^\circ, E_0 > 100 \text{ MeV}. \quad (1.27)$$

Chapter 1 Composition of Accelerator Radiation Fields

One can scale these results to other distances by using the inverse square law. It should be noted that one can get higher dose rates at 90° in certain circumstances due to the presence of softer radiation components. The forward intensity is a slowly varying function of target material except at very low Z . The angular full width, $\theta_{1/2}$, of the forward lobe (half-intensity) is approximately given by the relation due to Swanson (Sw79):

$$E_o \theta_{1/2} = 100 \text{ (MeV degrees)}. \quad (1.28)$$

Alternatively, according to Schopper et al. (Sc90) the average angle of emission is of the order of m_e/E_o (radians) where m_e is the rest mass of the electron.

Information about the bremsstrahlung photon spectrum is desirable. For thin targets ($X \ll X_o$), the spectrum of photons of energy k per energy interval dk , dN/dk , is approximated by;

$$\frac{dN}{dk} \approx \frac{X}{X_o k}. \quad (1.29)$$

Thick targets require consideration of the electromagnetic cascade. In general, the spectra fall as $1/k^2$ at $\theta = 0$ and even faster at larger angles (Sc79).

At higher energies ($E_o >$ approximately 100 MeV), the electromagnetic cascade development in accelerator components is very important and can result in a forward "spike" of photons with a characteristic angle of $\theta_c = 29.28/E_o$ (degrees, if E_o is in MeV). At $\theta = \theta_c$ the intensity of the spike has fallen to $1/e$ of its value at $\theta = 0$. This phenomena is important at electron storage rings and colliders.

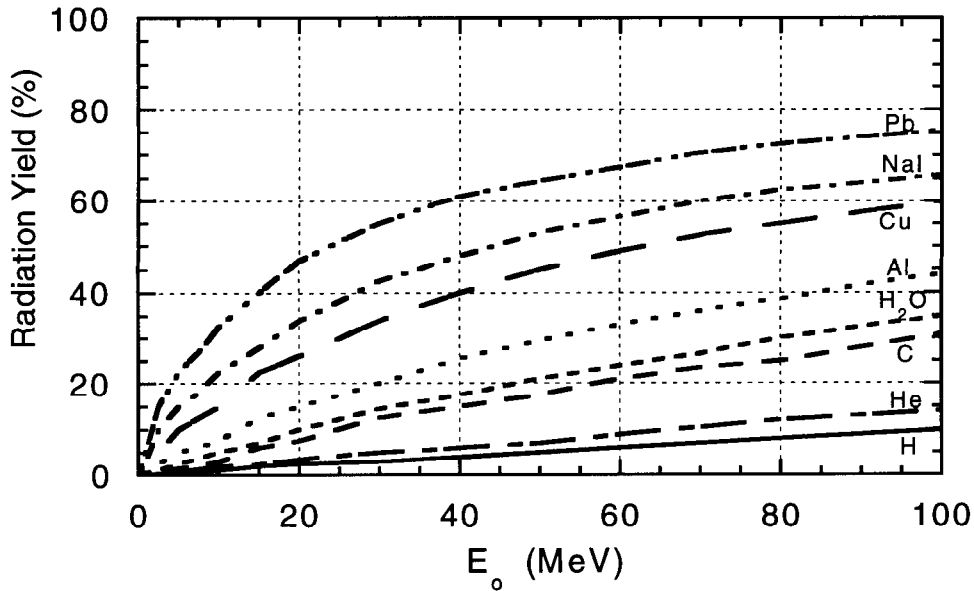


Fig. 1.7 Bremsstrahlung efficiency for electrons stopped in various materials. This is the fraction (in per cent) of the kinetic energy of incident electrons converted to radiation as a function of incident energy E_0 . The remainder is transferred to the medium by ionization. [Adapted from (Sw79)].

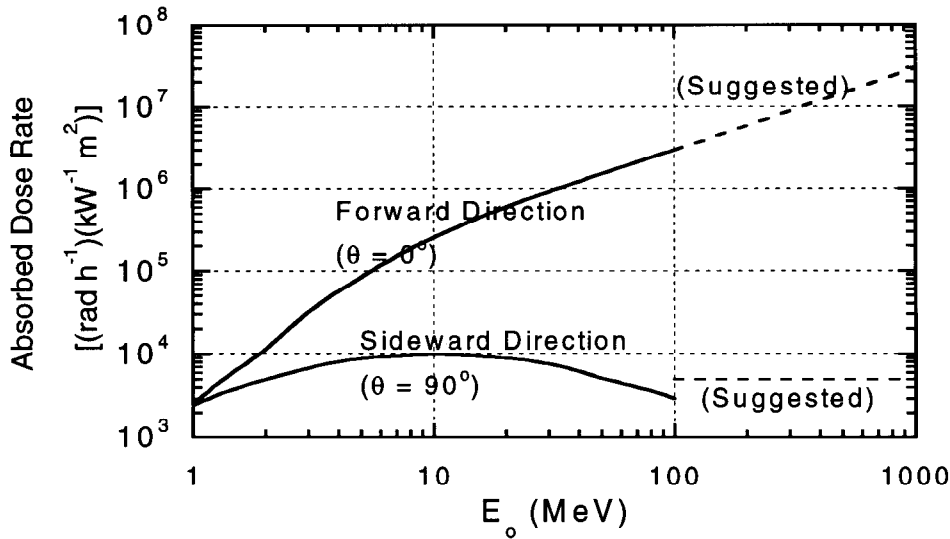


Fig. 1.8 Thick target bremsstrahlung from a high atomic number target. Absorbed dose rates at 1 meter per unit incident electron beam power (kW) are given as a function of incident electron energy E_0 . The dashed lines represent a reasonable extrapolation of the measured values. The dose rates measured in the sideward direction (smoothed for this figure) depend strongly on target and detector geometry and can vary by more than a factor of two. The dashed line at 90° represents the more penetrating radiation component to be considered in room shielding. [Adapted from (Sw79).]

Chapter 1 Composition of Accelerator Radiation Fields

Synchrotron radiation

Swanson (Sw90) presents a summary discussion of this important phenomenon. The movement of electrons in a circular orbit results in their centripetal acceleration. This gives rise to emission of photons. At nonrelativistic energies, this radiation is largely isotropic. However, for relativistic energies, a condition readily achievable for accelerated electron beams, the photons emerge in a tight bundle along a tangent to any point on a circular orbit. Figure 1.9 shows this bundle. The characteristic angle (i.e., the angle of $1/e$ of the zero degree intensity) of this "lobe" is

$$\theta_c = \frac{1}{\gamma} = \sqrt{1 - \beta^2} \text{ radians.} \quad (1.30)$$

The median energy of the power spectrum, ϵ_c , is given in terms of the total energy, W (GeV), and bending radius, R (meters) by:

$$\epsilon_c = \frac{2.218W^3}{R} \text{ (keV). [For protons, multiply by } (m_e/m_p)^3 \text{].} \quad (1.31)$$

The radiated power, P (watts) for a circulating electron current, I (milliamperes) is

$$P = \frac{88.46W^4 I}{R} \text{ [For protons, multiply by } (m_e/m_p)^4 \text{].} \quad (1.32)$$

More details on this subject, including the details of the angular distributions and spectra of the emitted photons, have been given in detail by Jackson (Ja75) with a good summary provided by the Particle Data Group (PDG96). Fig. 1.10 gives the universal radiation spectrum for high energies.

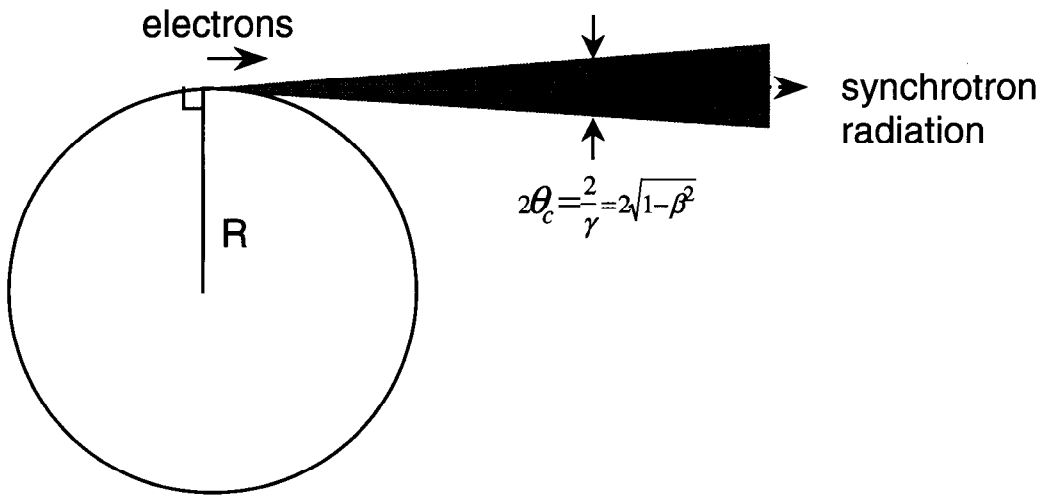


Fig. 1.9 Synchrotron radiation pattern for relativistic particles at the instantaneous location denoted by "electrons". Twice the opening angle, q_c , is shown as the cross-hatched region.

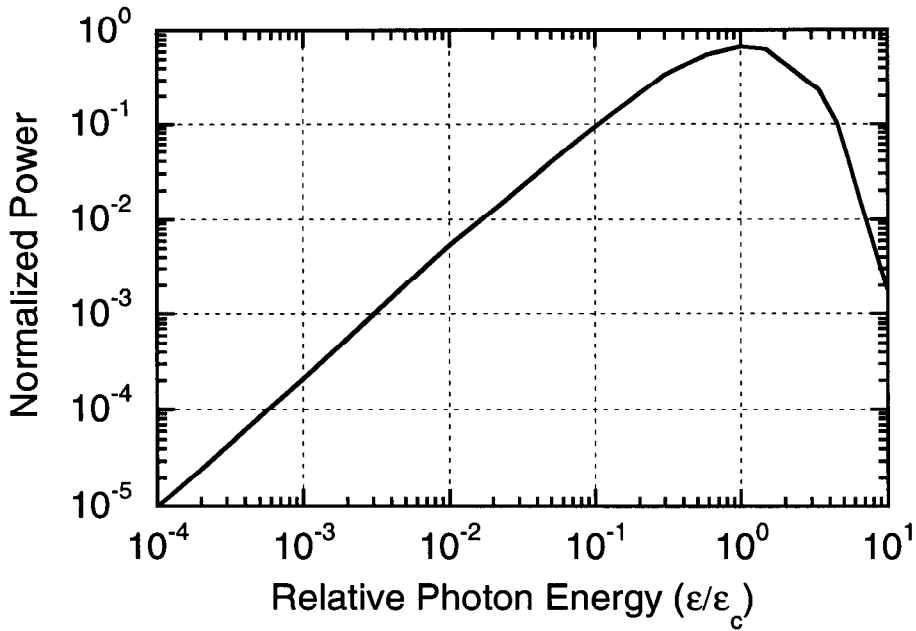


Fig. 1.10 Universal synchrotron radiation spectrum. The graph gives the relative power as a function of photon energy in units of characteristic energy, ϵ_c . It yields unity if integrated over all energies. [Adapted from (Sw83).]

Neutrons

Giant Photonuclear Resonance Neutrons

Neutron production can be expected to occur in any material irradiated by electrons or bremsstrahlung photons above the material-dependent threshold which varies from 10 to 19 MeV for light nuclei and 4 to 6 MeV for heavy nuclei. Thresholds of 2.23 MeV for deuterium and 1.67 MeV for beryllium are noteworthy exceptions. Between the threshold and approximately 30 MeV, a process known as the **giant photonuclear resonance** is the most important source of neutron emission from a material irradiated by electrons or photons. Swanson (Sw79) has given a detailed description of this process that is summarized here. A simple picture of this phenomenon is that the electric field of the photon transfers its energy to the nucleus by inducing an oscillation in which the protons as a group move oppositely to the neutrons as a group. This process has a broad maximum cross section at photon energies, $k_o = 20\text{-}23$ MeV for light nuclei for materials having mass numbers, A , less than about 40. For heavier targets, the peak is at an energy of approximately $k_o = 80A^{-1/3}$. It turns out that the yield, Y , of giant resonance neutrons at energies above approximately $2k_o$ is nearly independent of energy and nearly proportional to the beam power.

This process may be thought of as a process in which the target nucleus is excited and then decays somewhat later by means of neutron emission. It is a (γ, n) nuclear reaction as written in the scheme of notation in which the first symbol in the parentheses represents the incoming particle in a reaction while the second represents the outgoing particle. In this process the directionality of the incident electron or photon is lost so that these emissions are isotropic. Because of this isotropicity, the inverse square law may be used to estimate the flux density at any given distance, r . The spectrum of neutrons of energy E_n can be described as a Maxwellian distribution,

$$\frac{dN}{dE_n} = \frac{E_n}{T^2} \exp(-E_n / T), \quad (1.33)$$

where T is a *nuclear temperature* characteristic of the target nucleus and its excitation energy. T , in energy units, is generally in the range $0.5 < T < 1$ MeV. For this distribution, the most probable value of $E_n = T$ and the average value of $E_n = 2T$. This process generally dominates for kinetic energies $E_o < 150$ MeV. The excitation functions of total neutron yields in various materials are plotted in Fig. 1.11. Table 1.3 gives yields of giant resonance neutrons per watt of beam power ($\text{s}^{-1}\text{W}^{-1}$), the yield per GeV per sr ($Y_n \text{ GeV}^{-1} \text{ sr}^{-1}$), and a recommended dose equivalent source term ($\text{Sv cm}^2 \text{ GeV}^{-1}$). The agreement with various experiments is quite good according to Schopper et al. (Sc90). The last column is used in the following equation:

$$H = \frac{S_n}{r^2} E_o I, \quad (1.34)$$

Chapter 1 Composition of Accelerator Radiation Fields

where H is the dose equivalent in Sieverts, r is the radial distance from the target in cm, E_o is in GeV, and I is the total beam particles incident (e.g., during some time interval).

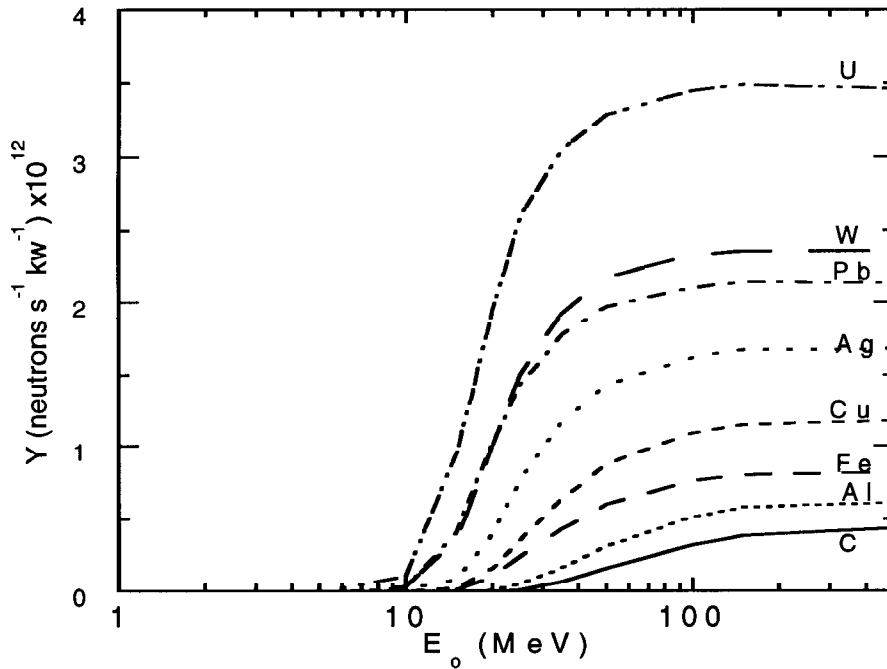


Fig. 1.11 Neutron yields from infinitely thick targets per kW of electron beam power as a function of electron beam energy E_o , disregarding target self-shielding. [Adapted from (Sw79b).]

Table 1.3 Yields and source terms of giant resonance neutrons in an optimum target geometry per incident ion at high energies ($E_o > 500$ MeV). [Adapted from (Sw79b) and (Sc90).]

Material	Total Neutron Production ($s^{-1}W^{-1}$)	Yield per GeV, steradian and electron, Y ($GeV^{-1}sr^{-1}$)	Recommended Source Terms ^a , S_n ($Sv\ cm^2\ GeV^{-1}$)
C	4.4×10^8	5.61×10^{-3}	4.3×10^{-12}
Al ^b	6.2×10^8	7.90×10^{-3}	6.0×10^{-12}
Fe	8.18×10^8	1.04×10^{-2}	7.7×10^{-12}
Ni	7.36×10^8	9.38×10^{-3}	6.9×10^{-12}
Cu	1.18×10^9	1.50×10^{-2}	1.1×10^{-11}
Ag	1.68×10^9	2.14×10^{-2}	1.5×10^{-11}
Ba	1.94×10^9	2.47×10^{-2}	1.8×10^{-11}
Ta	2.08×10^9	2.65×10^{-2}	1.8×10^{-11}
W	2.36×10^9	3.01×10^{-2}	2.0×10^{-11}
Au	2.02×10^9	2.58×10^{-2}	1.8×10^{-11}
Pb	2.14×10^9	2.73×10^{-2}	1.9×10^{-11}
U	3.48×10^9	4.44×10^{-2}	3.0×10^{-11}

^aTo get $Sv\ cm^2\ h^{-1}kW^{-1}$, multiply this column by 2.25×10^{16} .

^bThe value for aluminum is also recommended for concrete.

Quasi-Deuteron Neutrons

At energies above the giant resonance, the dominant neutron production mechanism is one in which the photon interacts with a neutron-proton pair within the nucleus rather than with the whole nucleus. The quasi-deuteron effect is so-named because for $E_o > 30$ MeV the photon wavelength is in resonance with the average inter-nucleon distance so that the photon interactions tend to occur with "pairs" of nucleons. Only neutron-proton pairs have a nonzero electric dipole moment, which makes interactions of photons with such pairs (pseudo-deuterons) favorable. This mechanism is important for $30 < E_o < 300$ MeV and has been described by Swanson (Sw79). The general effect of this mechanism is to add a tail of higher-energy neutrons to the giant resonance spectrum. For $5 < E_n < E_o/2$ (MeV), the nearly isotropic spectrum of quasi-deuteron neutrons is given by

$$\frac{dN}{dE_n} = E_n^{-\alpha} \text{ where, approximately, } 1.7 < \alpha < 3.6. \quad (1.35)$$

The slope becomes steeper as E_o , the kinetic energy of the incident electron, is approached. Eq. (1.35) is for *thin* targets, for *thick* target situations, the fall off with E_n is generally steeper. Since the mechanism is the (γ, np) reaction and the neutron and the proton are nearly identical in mass, they share the available energy equally so that the yield is essentially zero for $E_n > E_o/2$. In general, these neutrons are fewer in number and generally less important than are the giant resonance neutrons. Shielding against the latter will generally provide adequate protection against the former.

Neutrons Associated with the Production of Other Particles

There are interactions in which the production of other elementary particles, perhaps best typified by pions, becomes energetically possible at still higher energies ($E_o > 300$ MeV). These particles can then produce neutrons through secondary interactions as will be discussed in Chapter 3. DeStaebler (De65) has parameterized the measured yields of high energy particles per incident electron:

$$\frac{dY_n}{dEd\Omega} = \frac{7.5 \times 10^{-4}}{(1 - 0.75 \cos \theta)^2 A^{0.4}} \text{ (GeV}^{-1} \text{sr}^{-1}) \quad (1.36)$$

where A is the atomic mass (g/mol) of the target material. It is reasonable to use a dose equivalent conversion factor of approximately 1×10^{-13} Sv m² for these neutrons.

Muons

With electron beams, muons become of significance above an electron energy of approximately 211 MeV, the threshold of the process in which a μ^\pm pair is produced. They can, at much smaller fluxes, be produced by the decay of π^\pm and K^\pm which are, in turn, due to secondary production processes. Such decay muons will be discussed in more detail later. The muon rest energy is 105.7 MeV, its meanlife $\tau = 2.19 \times 10^{-6}$ s and the meanlife times the speed of light, $c\tau = 658.6$ m. These particles are highly forward peaked. The dose equivalent per fluence conversion factor, P , has been found by Stevenson (St73) to be 40 fSv m² (25,000 muons cm⁻² per mrem) for $100 \text{ MeV} < E_\mu < 200 \text{ GeV}$. At lower energies range-out of muons in the body with consequential higher energy deposition gives a conversion factor of 260 fSv m² (3850 muons cm⁻² per mrem). The results for a wide range of energies are included in Fig. 1.4.

A detailed theoretical treatment of muon production by incident electrons is given by Nelson (Ne68 and Ne74). Figure 1.12 gives the muon flux density as a function of energy at $\theta = 0^\circ$ while Fig. 1.13 shows an example of the angular dependence of these yields at $E_\mu = 20 \text{ GeV}$. The reasonableness of scaling with energy to larger values of E_0 is well-demonstrated.

Obviously, the range-energy relation of muons and considerations related to their energy loss mechanisms is relevant to shielding against muons regardless of the origin of the muons. Muons have very long mean ranges that are displayed in Fig. 1.14. At high energies ($E_\mu > 100 \text{ GeV}$), range straggling becomes severe (Va87). Also, above a critical energy for muons of several hundred GeV (in, say, iron), radiative losses begin to dominate such that the stopping power, dE/dx , is given by:

$$\frac{-dE}{dx} = a(E) + b(E)E \quad (1.37)$$

where $a(E)$ is the collisional ionization energy loss given by Eq. (1.15) ($\approx 0.002 \text{ GeV/gm cm}^{-2}$), and $b(E)$ is the radiative coefficient for E in GeV. The latter parameter is plotted in Fig. 1.15. The results presented here are also relevant relevant to further discussion in Chapter 3.

The mean range, R_μ , of a muon of kinetic energy E_0 , is approximated by

$$R_\mu \approx \frac{1}{b} \ln(a + bE_0). \quad (1.38)$$

Muon range straggling (Va87) is chiefly due to the fact that, above 100 GeV, electron-positron pair production, bremsstrahlung, and deep inelastic nuclear reactions become the dominant energy loss mechanisms. The cross sections for the latter two mechanisms are such that only a few interactions can be expected. Although these processes have low

Chapter 1 Composition of Accelerator Radiation Fields

probability, when they do occur they involve large energy losses and thus have quite significant effects. Tables 1.4 and 1.5 below give fractional energy loss and comparisons of muon ranges at high energies for different physical mechanisms. Here, the straggling is very important since shielding calculations based upon using the mean range values can lead to significant *underestimates* of the number of muons which can penetrate the shield.

Summary

Swanson (Sw79) has illustrated the broad features of the radiation field due to the interactions of electrons with no shielding that is given in Fig. 1.16. This figure is useful for making crude estimates of the resultant radiation field. As one can see, at all angles, from the standpoint of dose equivalent, the unshielded field is always dominated by photons. At small angles, the field is dominated by photons with muons as the next most important ingredient at TeV energies.

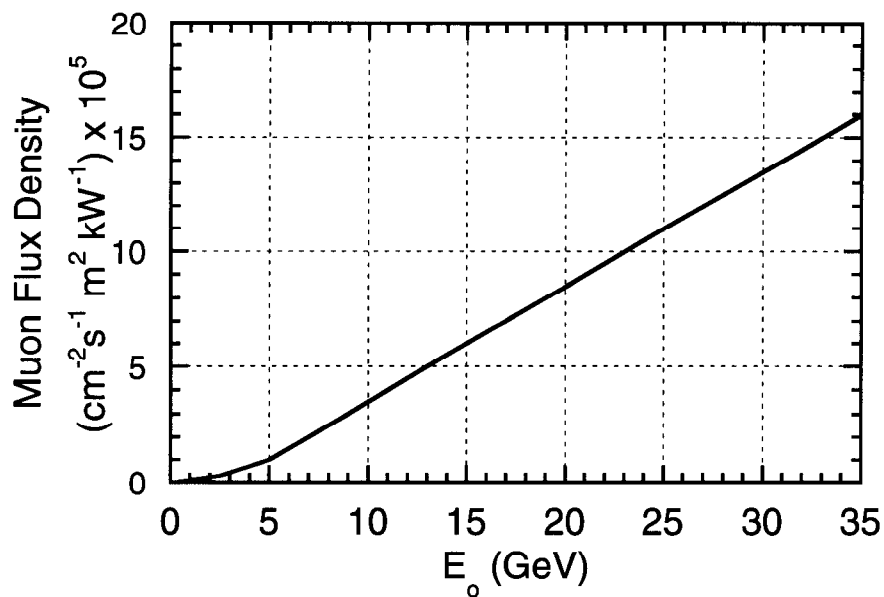


Fig. 1.12 Muon production at $\theta = 0^\circ$ from an unshielded thick iron target at one meter, as a function of electron energy, E_0 . [Adapted from (Sw79) and (Ne68).]

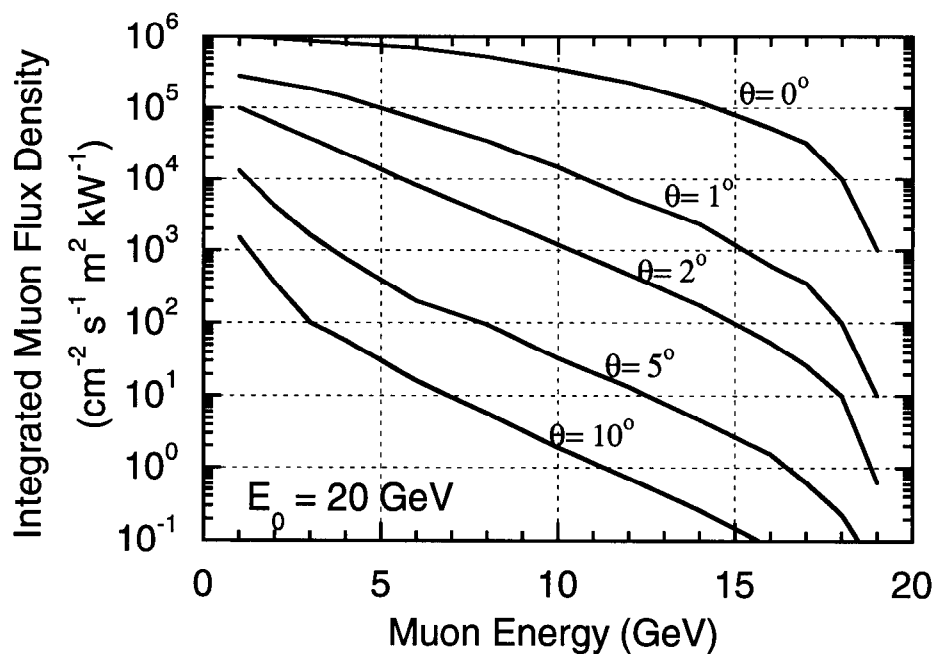


Fig. 1.13 Integrated muon flux density at 1 meter per kW of electron beam power as a function of muon energy for 20 GeV electrons incident on a thick iron target at several values of θ . The integral of the flux density over energy includes all muons that have energies that exceed the value of the abscissa at the given value of θ . [Adapted from (Ne68).]

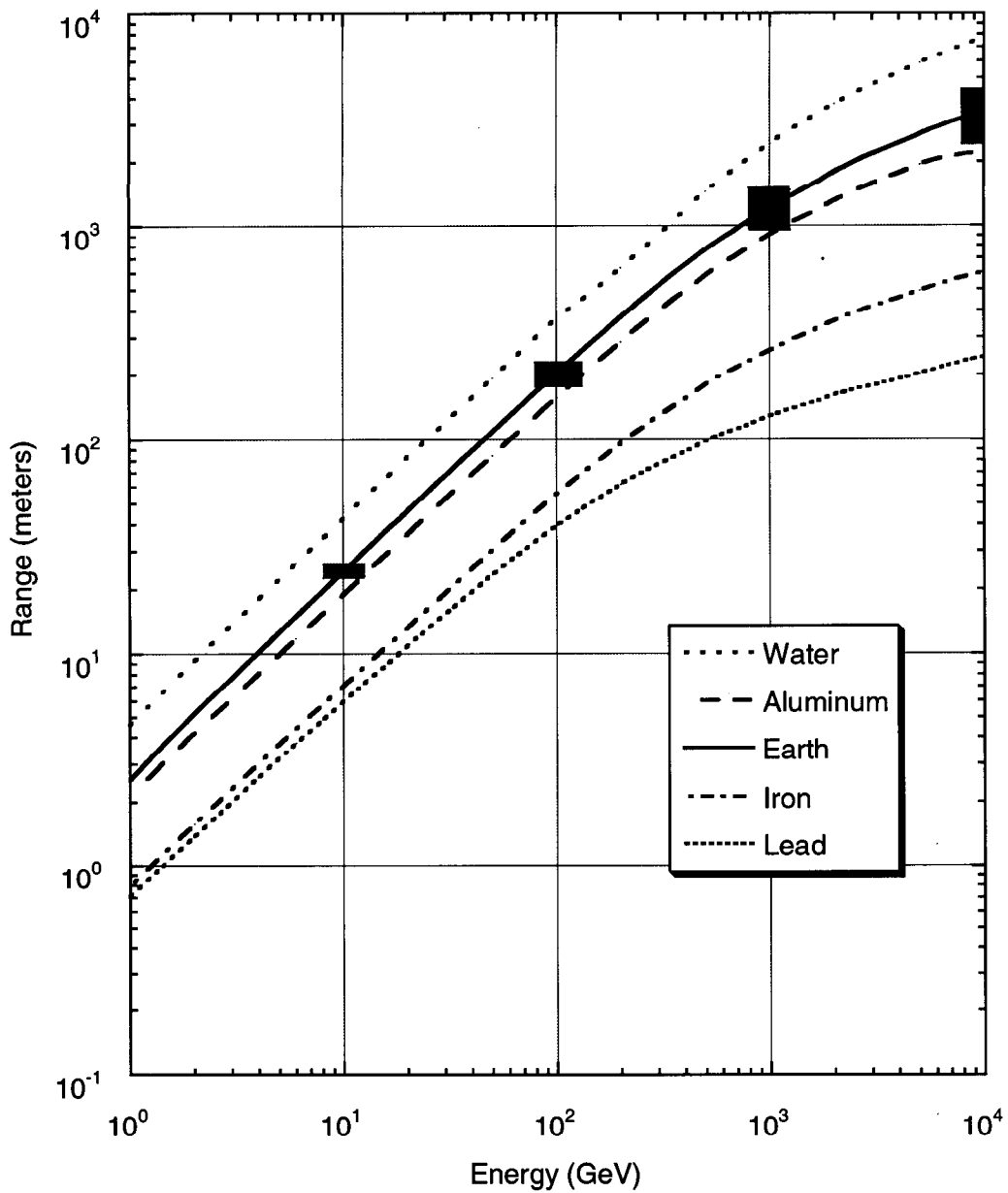


Fig. 1.14 Range-energy curves for muons in various materials. On the curve labeled "Earth", the gray boxes are indicative the approximate spread in the range due to straggling at one standard deviation at the indicated muon energy. The density of "earth" was taken to be 2.0 g cm^{-2} . The values were taken from (Sc90).

Chapter 1 Composition of Accelerator Radiation Fields

Table 1.4 Fractional energy loss of muons in soil ($\rho = 2.0 \text{ g cm}^{-3}$). The fractions of the total energy loss due to the four dominant energy loss mechanisms are given. [Adapted from (Va87).]

Energy (GeV)	Ionization	Brems-strahlung	Pair production	Deep inelastic nuclear scattering
10	0.972	0.037	8.8×10^{-4}	9.7×10^{-4}
100	0.888	0.086	0.020	0.0093
1000	0.580	0.193	0.168	0.055
10,000	0.167	0.335	0.388	0.110

Table 1.5 Comparison of muon ranges (meters) in heavy soil ($\rho = 2.24 \text{ g cm}^{-3}$) [Adapted from (Va87)]

Energy (GeV)	Mean Ranges from dE/dx in Heavy Soil (meters)				
	Mean Range (meters)	Standard Deviation (meters)	All Processes	Coulomb Losses Only	Coulomb & Pair Production Losses
10	22.8	1.6	21.4	21.5	21.5
30	63.0	5.6	60.3	61.1	60.8
100	188	23	183	193	188
300	481	78	474	558	574
1000	1140	250	1140	1790	1390
3000	1970	550	2060	5170	2930
10,000	3080	890	3240	16700	5340
20,000	3730	1070			

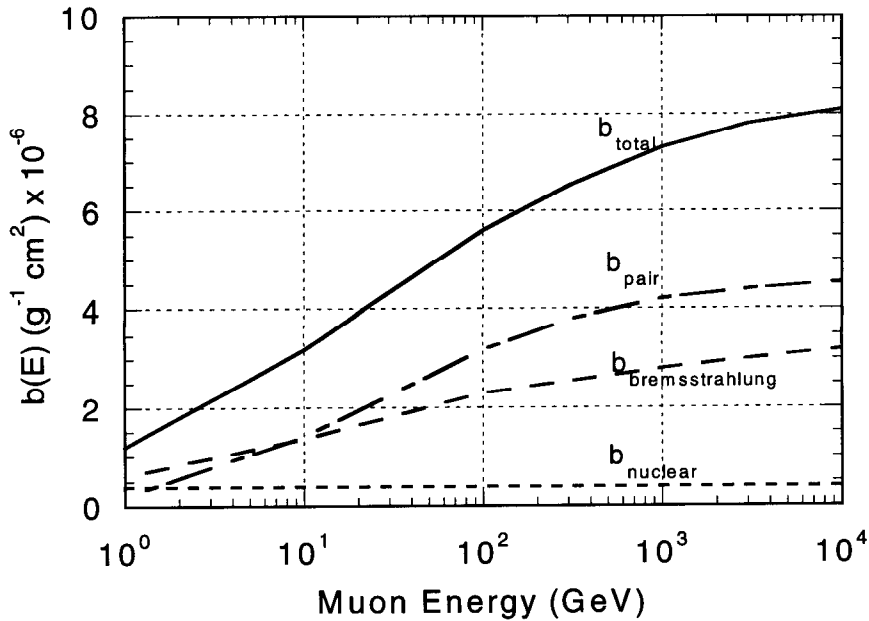


Fig. 1.15 Contributions to the fractional energy loss by muons in iron due to e^+e^- pair production, bremsstrahlung, and photonuclear interactions. See Eq (1.37). [Adapted from (PDG96).]

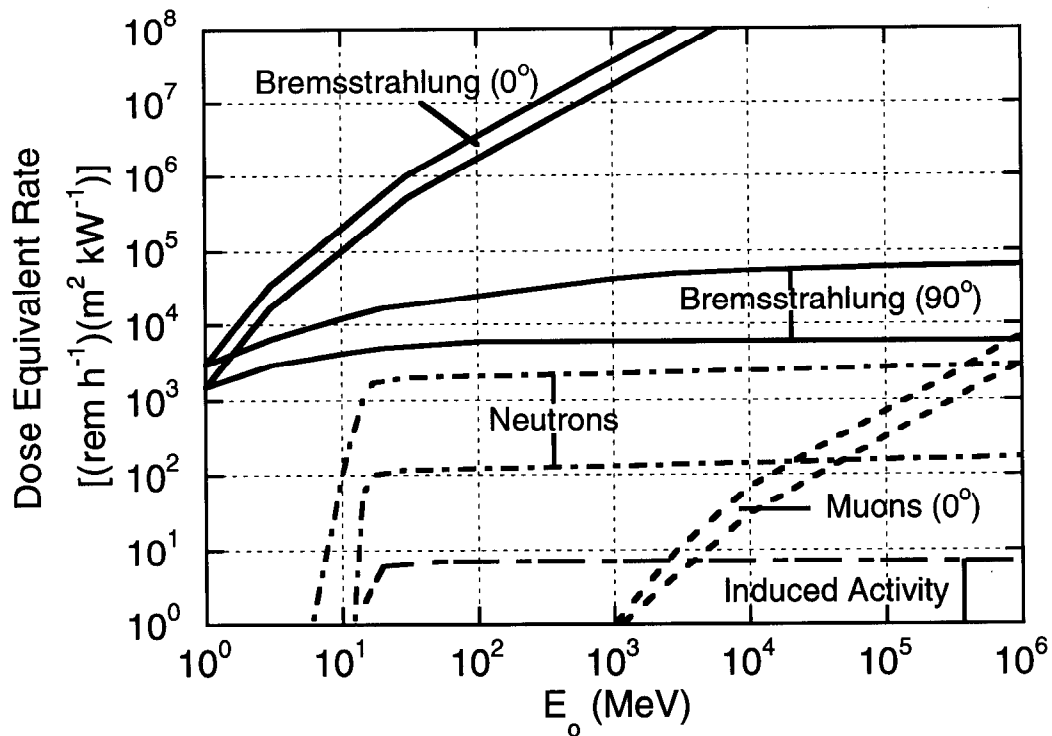


Fig. 1.16 Dose-equivalent rates per unit primary beam power at one meter produced by various types of "secondary" radiations from a high-Z target as a function of primary beam energy, if no shielding were present (qualitative). The width of the bands suggests the degree of variation found, depending on such factors as target material and thickness. The angles at which the various processes are most important are indicated. [Adapted from (Sw79).]

V. Radiation Production by Proton Accelerators

The Direct Beam

Direct beams at proton accelerators, from the dosimetric standpoint, nearly always dominate over any type of secondary phenomena since the beam current is generally confined to small dimensions. Figure 1.4 includes the dose equivalent per fluence as a function of proton energy. The physical reason that the conversion factor shows such a prominent transition at about 200 MeV is that below that energy the proton range in tissue is less than the thickness of the human body. Hence as the energy is increased above 200 MeV, the energy largely escapes from the body so that it requires a far larger fluence of protons to deliver the same dose equivalent.

As the energy of a proton beam increases, the range of the protons increases to where the probability of the proton interacting before it has lost all of its energy due to ionization in a target gradually becomes significant. Tesch has summarized this and the results are shown in Fig. 1.17 for various materials and energies (Te85).

Neutrons (and other hadrons at high energies)

$E_o < 10 \text{ MeV}$:

For nuclear reactions, the **Q-value**, Q_v , is defined in terms of the rest masses, m_i ,

$$Q_v = [(m_1 + m_2) - (m_3 + m_4)]c^2 \quad (1.39)$$

for nuclear reaction symbolized by $m_1 + m_2 \rightarrow m_3 + m_4$ which is generally denoted $m_2(m_1, m_3)m_4$. $Q_v > 0$ implies an **exothermic** nuclear reaction. **Endothermic** ($Q_v \leq 0$) reactions are characterized by a **threshold energy**, E_{th} , given by:

$$E_{th} = \frac{m_1 + m_2}{m_2} |Q_v|. \quad (1.40)$$

Below 10 MeV, (p,n) reactions are important for some materials because these reactions commonly have very low thresholds ($< 5 \text{ MeV}$). Many features are highly dependent upon the details of the structure of the target nuclei and are often sensitive to the target element, angle, and energy. For example, ${}^7\text{Li}(p,n){}^7\text{Be}$ has a threshold of 1.9 MeV and the reaction cross section, σ , quickly rises to a value of 300 mb.

$10 < E_o < 200 \text{ MeV}$

For protons having energies of this magnitude and higher, neutrons are usually the dominant feature of the radiation field that results from their interactions. In this region of energy, the yields are smoother functions of energy due to the lack of resonances, but are also more forward-peaked. Tesch (Te85) has summarized the total yields per incident

Chapter 1 Composition of Accelerator Radiation Fields

proton for different materials as a function of energy in Fig. 1.18. In this figure the smooth curves agree with the original primary data to within about a factor of two. An important feature is that for $50 < E_o < 500$ MeV, $Y \propto E_o^2$ while for $E_o > 1$ GeV, $Y \propto E_o$. Especially at the lower energies, many of the neutrons produced are so-called "evaporation" neutrons that would have an isotropic distribution. Further discussion of angular distribution effects for the so-called "cascade" neutrons follows later.

In this region there are extensive angular distribution data as a result of nuclear physics research. The general feature is that the distributions are forward-peaked. Representative examples of angular distributions of neutrons are given in Figs. 1.19 and 1.20 for 52 and 200 MeV protons, respectively.

200 MeV < E_o < 1 GeV; ("intermediate" energy):

In this region, many more reaction channels become open and the number of protons emitted gradually becomes approximately equal to the number of neutrons. In fact, at the highest energies for such unshielded conditions, the radiation effects of protons and neutrons are essentially identical and both must be taken into account. Thus reliance on the values in Fig. 1.18 could underestimate radiation effects by as much as a factor of two.

E_o > 1 GeV ("high" energy region):

In this region, both the calculations and measurements become much more difficult. Often, "threshold" detectors are used to detect neutrons above some reaction threshold energy. Figures 1.21, 1.22, 1.23, and 1.24 show representative data at 14, 26, 22, and 225 GeV, respectively. These results should be regarded as thin target values. "Thin" target in this context means a target shorter than the **mean free path** for **removal** of the high energy protons. Table 1.6 summarizes common removal mean free paths. Considerable efforts have been made to semi-empirically fit the distributions of the yields of secondary particles produced by proton interactions. These efforts are needed to supply the needs of the particle physics community as well as to address radiation safety issues. They began in the early days of radiation protection and continue to the present and are embodied in the continual development of Monte-Carlo programs designed to calculate the properties of hadronic cascades (see Chapter 3). As an example of a particularly successful early model, Ranft (Ra66) developed the following formula for the yield of protons (or neutrons), which when integrated numerically above the indicated particle threshold, well describes the experimental data presented in Figs. 1.21 and 1.22, according to Patterson and Thomas (Pa73):

$$\frac{d^2Y}{d\Omega dp} = \left\{ \frac{A}{p_o} + \frac{Bp}{p_o^2} \left[1 + a \left\{ 1 - \frac{p_o}{p} \right\} \right] \right\} \times \left\{ 1 + a \left[1 - \frac{pp_o}{m^2} \right] \right\} p^2 \exp(-Cp^2\theta),$$

(protons or neutrons sr⁻¹ GeV⁻¹ per interacting proton) (1.41)

Chapter 1 Composition of Accelerator Radiation Fields

where

p_o is the primary proton momentum (GeV/c)
 m is the proton rest energy (GeV/c²)
 $a = \{1 + (p_o/m)^2\}^{1/2}$
 θ is the production angle (radians).

The parameters A , B , and C are material dependent and are given in Table 1.7

For simple radiation protection calculations, Sullivan (Su89) has developed a formula for the fluence, $\Phi(\theta)$, of hadrons with $E_o > 40$ MeV that will be produced at one meter from a copper target struck by protons in the energy region $5 < E_o < 500$ GeV per interacting proton:

$$\Phi(\theta) = \frac{1}{2\left[\theta + \left(35/\sqrt{E_o}\right)\right]^2} \quad (\text{cm}^{-2} \text{ per interacting proton}), \quad (1.42)$$

where E_o is in GeV and θ is in degrees.

This formula also adequately accounts for the distributions of neutrons per incident proton in the region of incident proton energy $0.025 < E_o < 1$ GeV if it is multiplied by, approximately, a factor of two. This equation is plotted in Fig. 1.25, for "lateral" ($\theta \approx 90^\circ$) and "forward" ($\theta \approx 0^\circ$) directions.

Of course, the dose equivalent is more directly germane to radiation protection concerns than is the "raw" fluence. In principal, the dose equivalent can be obtained by integrating over the spectrum,

$$H = \int_0^{E_{\max}} P(E)\Phi(E)dE, \quad (1.43)$$

or by summation, taking into account the "coarseness" of available data and/or calculations:

$$H = \sum_{j=1}^m P_j(E)\Phi_j(E)\Delta_j(E). \quad (1.44)$$

Tesch (Te85) has done this to obtain the dose equivalent at one meter from a copper target ($\theta = 90^\circ$) bombarded by protons of various energies. The result is plotted in Fig. 1.26. Above about 1 GeV, the dose equivalent is approximately proportional to E_p . Levine (Le72) has measured the angular distribution of absorbed dose for 8 and 24 GeV/c protons incident on a Cu target. The results are in approximate agreement with those found by Tesch.

Chapter 1 Composition of Accelerator Radiation Fields

Table 1.6 Summary of removal mean free paths for protons

Material	Density (grams/cm ³)	Removal Mean Free Path (grams/cm ²)	Removal Mean Free Path (cm)
hydrogen gas	9.00 X 10 ⁻⁵	43.3	4.81 X 10 ⁵
beryllium	1.85	55.5	30.03
carbon	2.27	60.2	26.58
aluminum	2.70	70.6	26.15
iron	7.87	82.8	10.52
copper	8.96	85.6	9.55
lead	11.35	116.2	10.24
uranium	18.95	117.0	6.17
air	1.29 X 10 ⁻³	62.0	4.81 X 10 ⁴
water	1.00	60.1	60.10
concrete(typical)	2.50	67.4	26.96
silicon dioxide (quartz)	2.64	67.0	25.38
plastics (polyethylene)	0.93	56.9	61.51

Table 1.7 Material-dependent parameters to be used in Eq. 1.41 (from Ra67)

Target	A	B	C
H ₂	0.55	-0.30	2.68
Be	0.68	-0.39	3.12
Fe	0.92	-0.75	2.90
Pb	1.14	-1.06	2.73

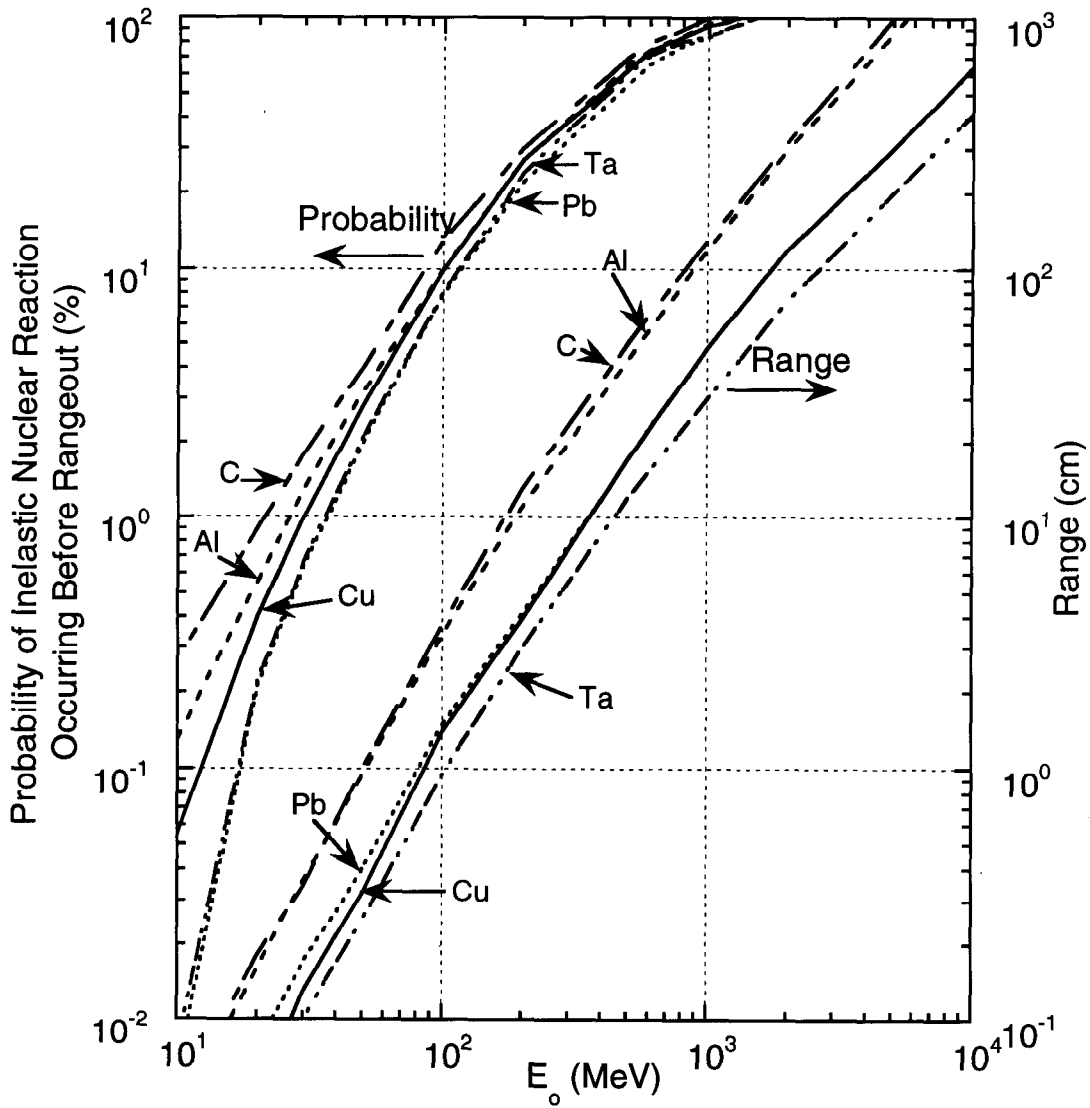


Fig. 1.17 Range of protons (curves on right and right hand scale) and probability of inelastic nuclear interaction within the range (curves on left and left hand scale) for various materials [Adapted from (Te85).]

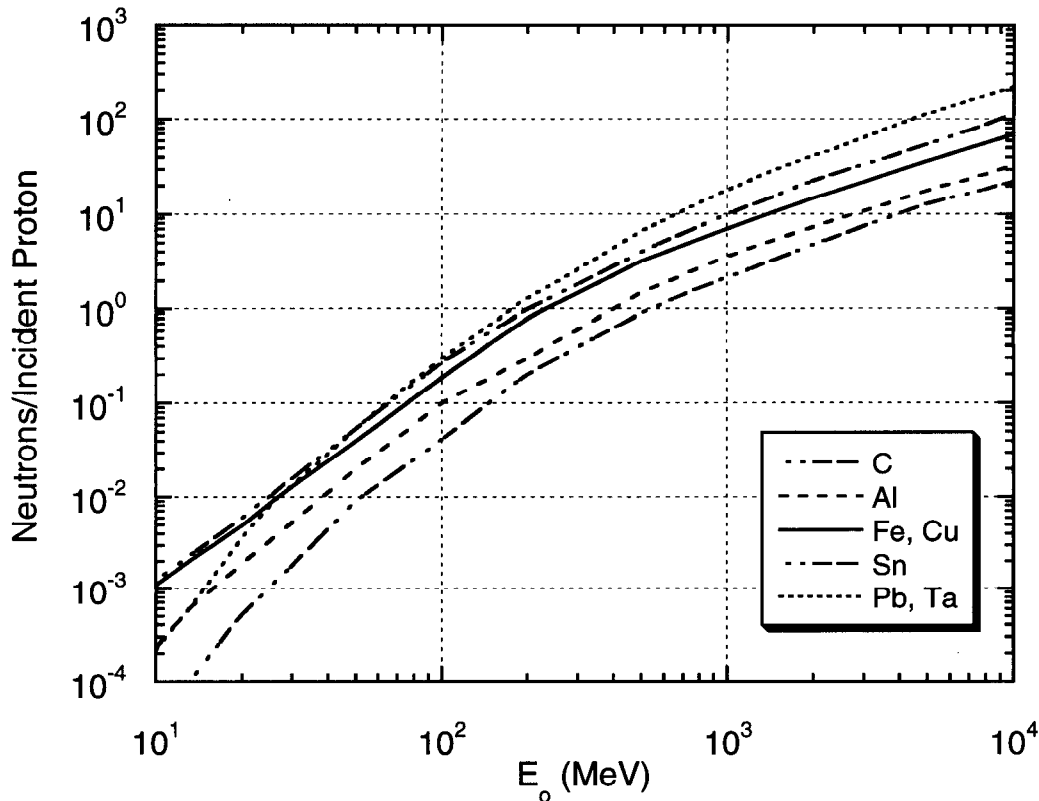


Fig. 1.18 Total neutron yield per proton for different target materials as a function of incident proton energy, E_0 . [Adapted from (Te85).]

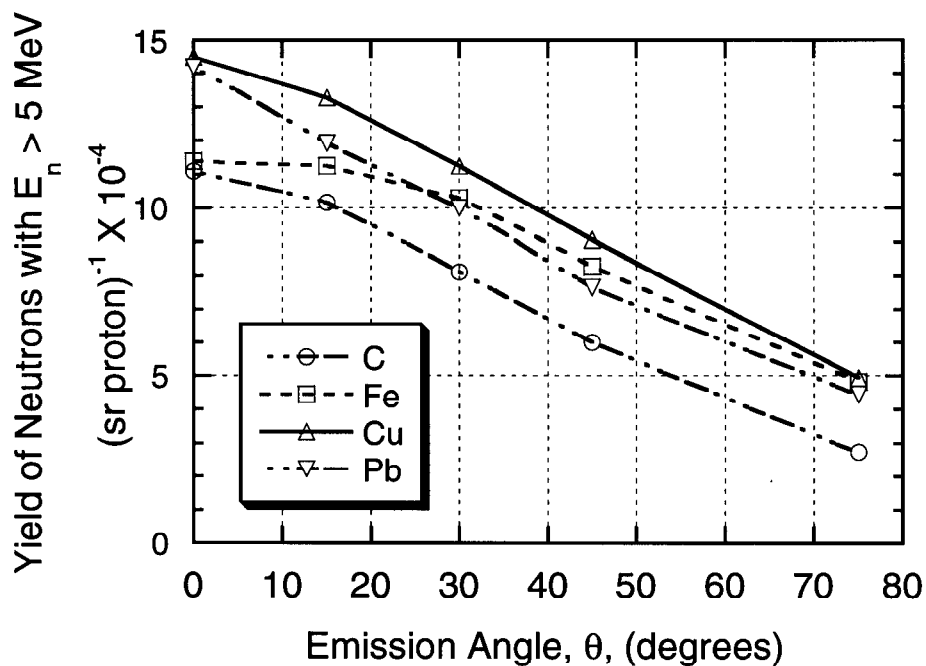


Fig. 1.19 Measured angular distributions of total neutron yield above 5 MeV for carbon, iron, copper, and lead bombarded by 52 MeV protons. The measurements were normalized at $\theta = 15^\circ$. The curves are drawn to guide the eye. [Adapted from (Na78).]

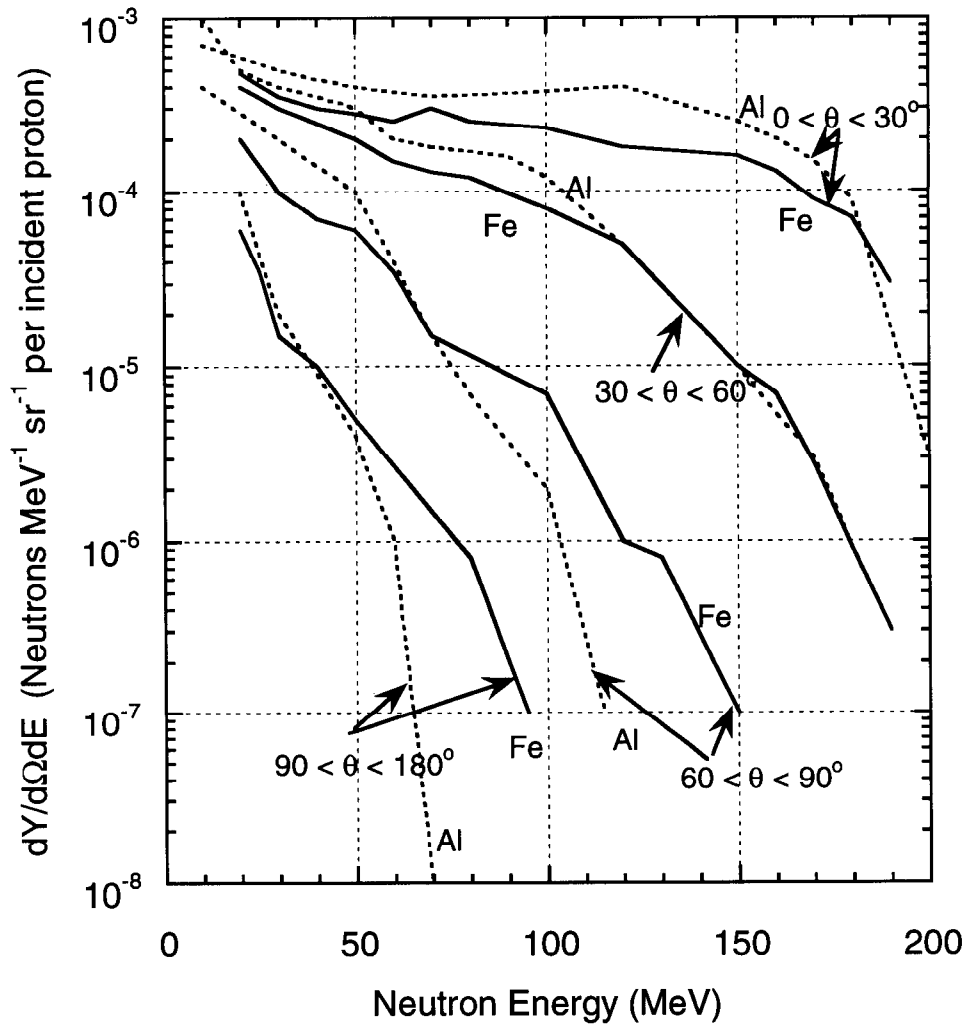


Fig. 1.20 Calculated energy spectra of neutrons emitted by iron and aluminum targets bombarded by 200 MeV protons for four ranges in θ . The iron calculations are from (Ha88) while the aluminum results are from (Al75). [Adapted from (Ha88).]

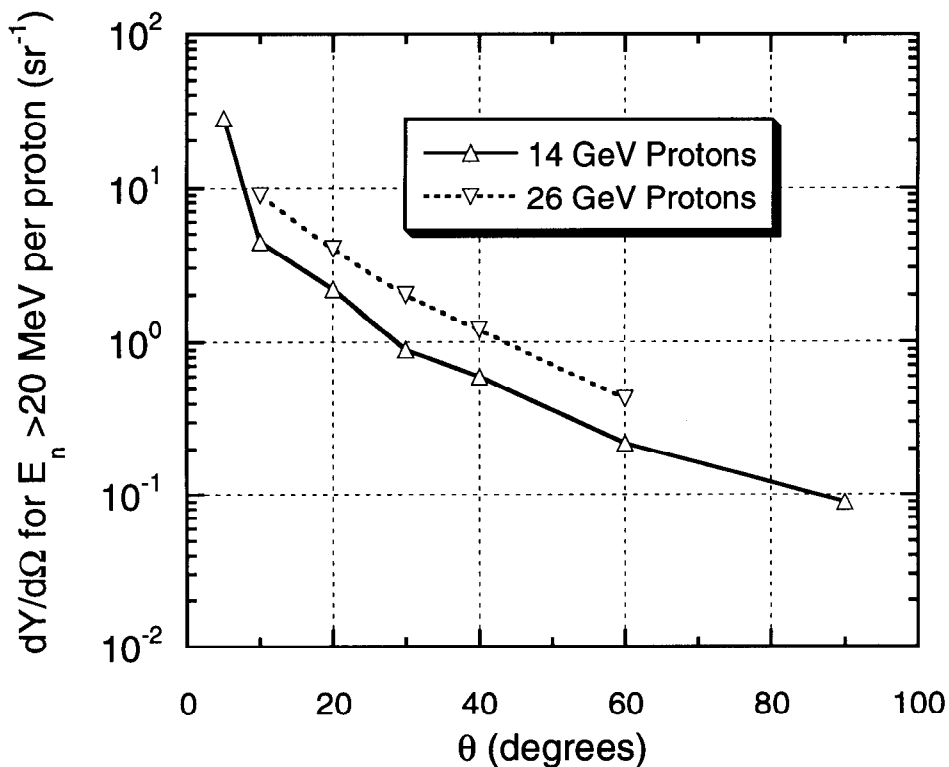


Fig. 1.21 Measurements of the angular distribution, $dY/d\Omega$, of neutrons above 20 MeV produced by 14 and 26 GeV protons on a thin beryllium target. The yield is per interacting proton. The lines are drawn to guide the eye. [Adapted from (Gi68).]

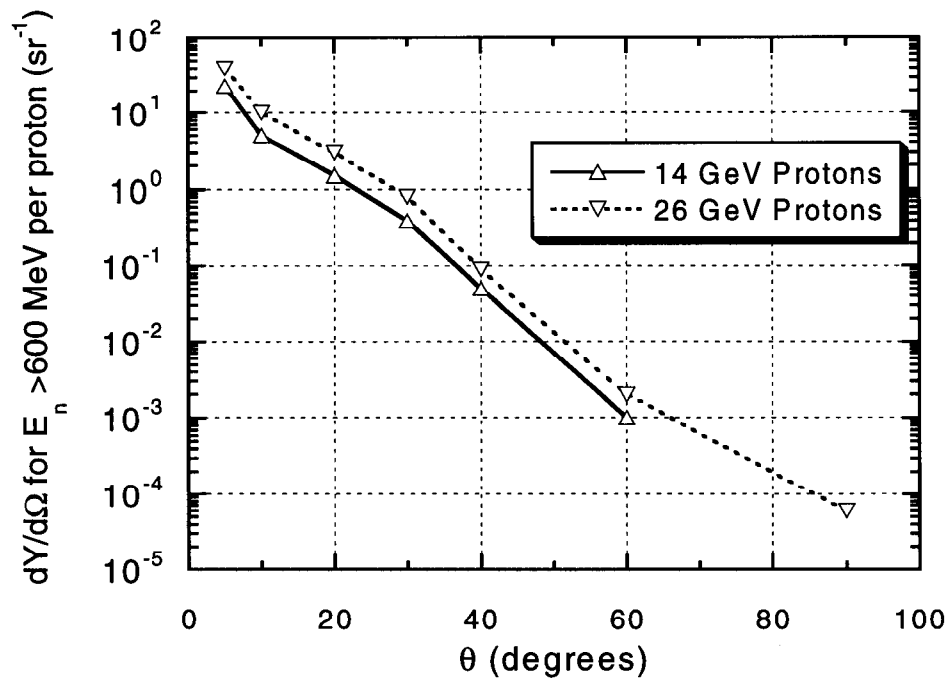


Fig. 1.22 The angular distribution, $dY/d\Omega$, of neutrons above 600 MeV produced by 14 and 26 GeV protons on a thin beryllium target. The yield is per interacting proton. The lines are drawn to guide the eye [Adapted from (Gi68).]

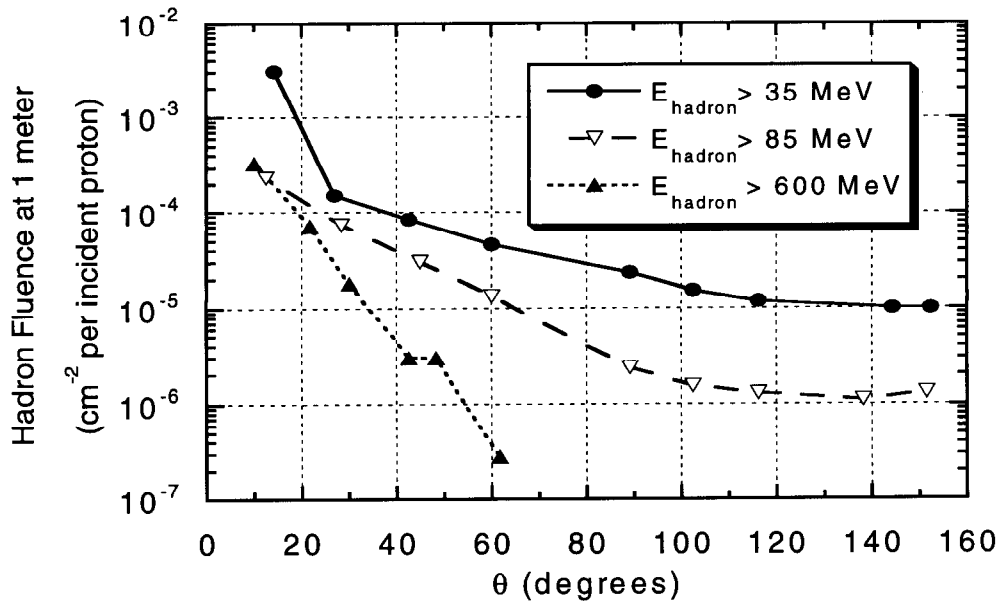


Fig. 1.23 Measured angular distributions of hadron fluence (particles cm^{-2}) at 1 meter from a copper target bombarded by 22 GeV protons. Several choices of hadron energy thresholds are shown. [Adapted from (Ra72).]

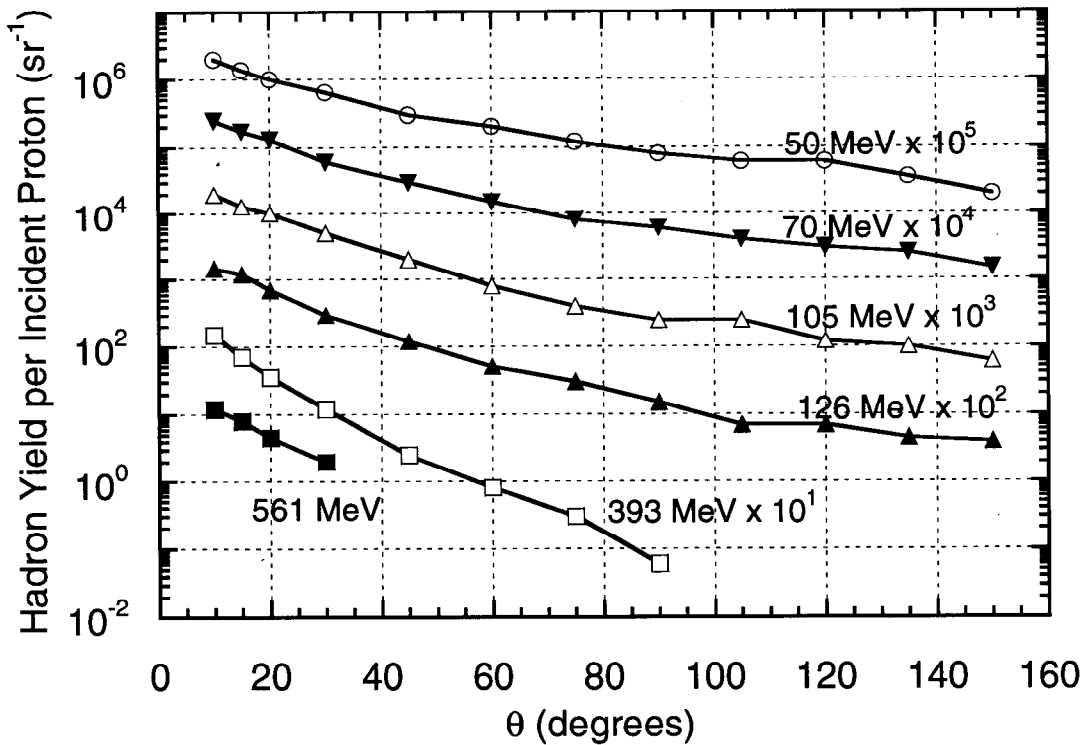


Fig. 1.24 Measurements of hadron yields above different energy thresholds as a function of production angle θ around a 15 cm long copper target bombarded by 225 GeV protons. The data have been multiplied by the indicated factors prior to plotting. The lines are intended to guide the eye. [Adapted from (St85).]

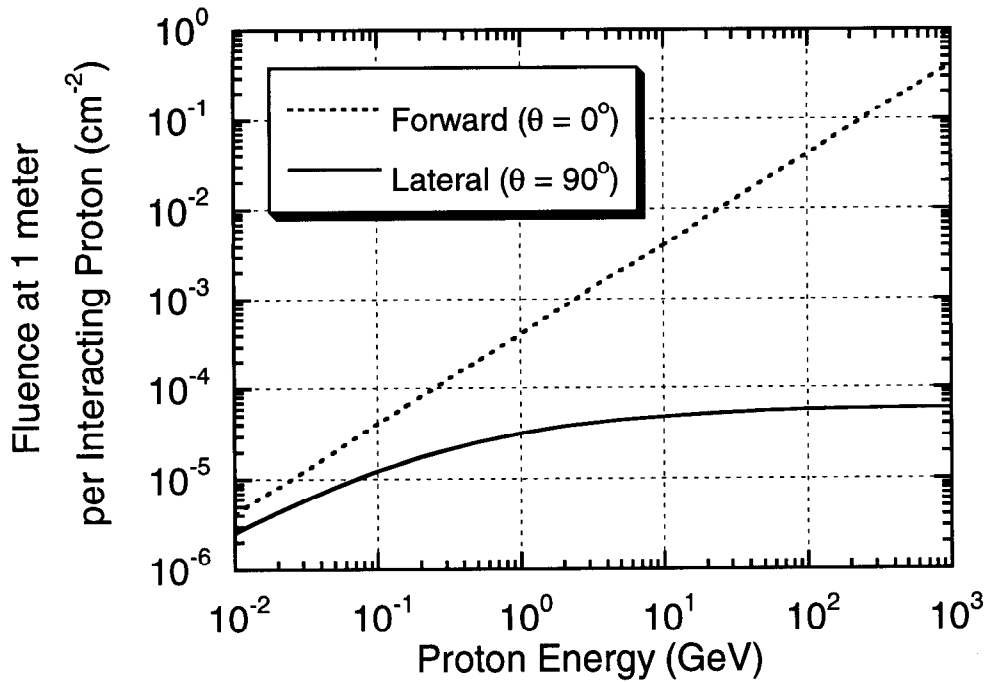


Fig. 1.25 Fluence of hadrons exceeding 40 MeV in energy, per interaction, at 1 meter from the target in both the forward ($\theta = 0^\circ$) and sideways ($\theta = 90^\circ$) direction as a function of the interacting proton energy. The proton is interacting in a copper target. [According to (Su89).]

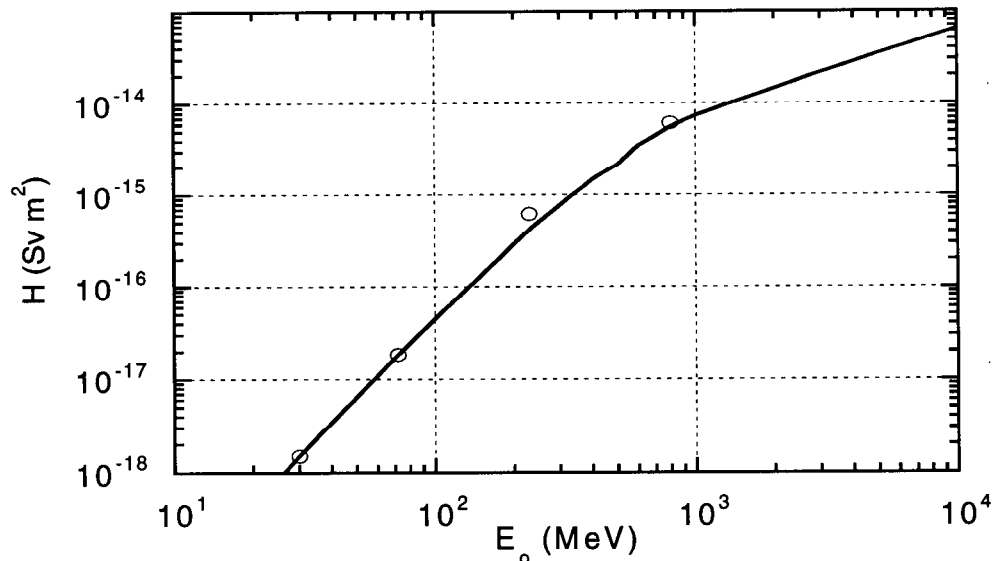


Fig. 1.26 Dose equivalent per proton due to neutrons at $\theta = 90^\circ$ with energies higher than 8 MeV at a distance of 1 meter from a copper target. The curve is an interpolation between the normalized experimental measurements denoted by the open symbols. [Adapted from (Te85).]

Chapter 1 Composition of Accelerator Radiation Fields

Muons

Muons at proton accelerators arise from two principal mechanisms. Production by pion and kaon decay are outlined as follows where mass of the parent particles, the branching ratio (the percentage of time the parent particle decays by the reaction given), the meanlife, τ , and the value of $c\tau$ (PDG96) are also given:

$$\pi^{\pm} \rightarrow \mu^{\pm} + \nu_{\mu}; m_{\pi} = 139.6 \text{ MeV}, \tau = 2.60 \times 10^{-8} \text{ s}, (99.99 \% \text{ branch}),$$

($c\tau = 7.804 \text{ m}$), and

$$K^{\pm} \rightarrow \mu^{\pm} + \nu_{\mu}; m_K = 493.7 \text{ MeV}, \tau = 1.24 \times 10^{-8} \text{ s}, (63.51 \% \text{ branch}),$$

($c\tau = 3.713 \text{ m}$).

The other important muon production mechanism associated with incident high energy protons is so-called "direct" muon production that will be discussed in more detail in Chapter 3.

At proton and ion accelerators the production of muons is generally dominated by a tertiary effect due to the decay of secondary particles. Muon fields are forward-peaked and, normally, dominated by those from pion decay (except, perhaps at the highest energies). Usually, Monte-Carlo techniques are needed to accurately estimate muon intensities. This is because of the need to:

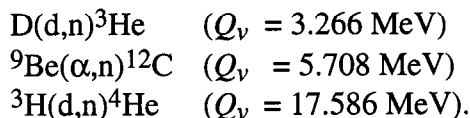
- A. calculate the production of pions from the proton interactions,
- B. follow the pions until they decay or interact,
- C. adequately account for the range-energy relation and range straggling,
- D. track the muons to the point of interest, for example, through magnetic fields.

VI. Primary Radiation Fields at Ion Accelerators

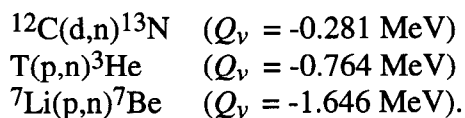
Because the ionization range for ions of a given kinetic energy decreases as a function of ion mass, targets become effectively "thicker" as the ion mass increases.

light ions (ion mass number, $A < 5$)

For such ions there are exothermic reactions that should be treated as "special cases". Noteworthy examples (followed by their reaction Q-values, Q_v , in parentheses) are:



In some cases monoenergetic beams of neutrons are possible using these or the following slightly endothermic reactions:



The energies of such neutrons can range from 0 to 27 MeV for bombarding energies up to 10 MeV.

In general, deuteron stripping and breakup reactions [(d,n)] have the highest yields because the binding energy of the deuteron is only 2.225 MeV. One gets an extra neutron "for free"! This phenomenon is especially pronounced at the lower energies. In the low energy region, and especially with light ions, one should carefully consider all possible reactions given the materials present in conjunction with the ions that are being accelerated. Patterson and Thomas (Pa73) have summarized total neutron yields for light ions. In general, the yields for the various light ions behave similarly to those due to protons. That is, the yield is within, typically, a factor of three of that expected for proton beams. A good measurement of neutron yields from 40 MeV α -particles has been provided by Shin et al (Sh95). Some high energy neutron production data for 640 and 710 MeV α -particles has been provided by Cecil et al. (Ce80).

heavy ions (ions with $A > 4$)

At higher energies and especially at higher masses, neutron yield and dose equivalent data and calculations are very sparse. The data is usually normalized in terms of kinetic energy per atomic mass unit (**specific energy**), expressed in units of MeV/amu, or kinetic energy per nucleon because reaction parameters generally scale to that parameter. In the literature the technical distinction between energy/amu and energy/nucleon is often ignored. In the range up to 20 MeV/amu, Ohnesorge, et al (Oh80) have measured dose equivalent rates at one meter at $\theta = 90^\circ$ from thick targets of iron, nickel, or copper

Chapter 1 Composition of Accelerator Radiation Fields

bombarded by ^4He , ^{12}C , ^{14}N , ^{16}O , and ^{20}Ne beams. The dose equivalent was found to be essentially independent of ion type as a function of specific energy. At 10 MeV/amu, a value of 6.3×10^{-18} Sv/incident ion while at 20 MeV/amu, a value of 3.6×10^{-17} Sv/incident ion was measured. Other data in this general energy regime are exemplified by that of Hubbard et al (Hu60), and Aleinikov, et al (Al85).

Tuyn et. al (Tu84) reports studies done with 86 MeV/amu ^{12}C ions incident on Fe targets slightly thicker than one range. The measurements are shown in Fig. 1.27. At a specific energy of 155 MeV/amu, Britvich et al (Br98) have measured energy spectra and total neutron yields and angular distributions for ^4He , ^{12}C , and ^{16}O ions stopping in a thick target of an alloy of tungsten, nickel, and copper commonly known as "Hevimet". The differential yields, $dY/d\Omega$, were fit by the form,

$$\frac{dY}{d\Omega} = C \exp(-\beta\theta), \quad (1.45)$$

with the total yields being found by the integration,

$$Y_{total} = 2\pi \int_0^\pi d\theta \sin\theta \frac{dY(\theta)}{d\Omega} = 2\pi C \frac{(e^{-\beta\theta} + 1)}{(\beta^2 + 1)}. \quad (1.46)$$

The results are presented in Fig. 1.28. The total neutron yield for ^4He , ^{12}C , and ^{16}O was found to be 4.90, 1.56, and 1.74 neutrons/incident ion, respectively.

Clapier and Zaidins (Cl83) have surveyed the existing data from 3 to 86 MeV/amu and have been able to fit the fluence angular distribution follows the following functional form:

$$\Phi(\theta, \xi) \approx \frac{1}{4\pi} \left[\frac{1}{\ln\{1 + 1/\xi\}} \right] \left[\frac{1}{\xi + \sin^2(\theta/2)} \right] \quad (1.47)$$

where θ is in degrees and the fitting parameter ξ is determined by

$$\xi = \frac{\Phi(90^\circ)}{\Phi(0^\circ) - \Phi(90^\circ)} = \frac{1}{\Phi(0^\circ)/\Phi(90^\circ) - 1}, \quad (1.48)$$

and where $\Phi(\theta, \xi)$ is the fluence or dose equivalent at θ . These same authors have found that the total yield, Y (neutrons/ion) can be approximately fit as a function of the projectile atomic number, Z , and the specific energy, W (MeV/amu). They found essentially no dependence on atomic number of the target. The expressions that result are:

Chapter 1 Composition of Accelerator Radiation Fields

$$Y = (W, Z) = C(Z)W^{\eta(Z)} \quad \text{with} \quad (1.49)$$

$$\eta(Z) = 1.22\sqrt{Z} \quad \text{and} \quad (1.50)$$

$$C(Z) = \frac{1.95 \times 10^{-4}}{Z^{2.75}} \exp\{-0.475(\ln Z)^2\} \quad (1.51)$$

These authors have tabulated the values of the parameters $C(Z)$ and $\eta(Z)$ in Table 1.8. They also give a few examples of the parameter, ξ , in the expression for fitting the angular distribution. They report values of 0.07 for uranium incident on uranium at 9 MeV/amu, 0.025 for neutrons of energy < 20 MeV produced by 86 MeV/amu ^{12}C incident on iron, and 3×10^{-4} for neutrons of energy > 20 MeV produced by 86 MeV/amu ^{12}C incident on iron. One could use values given in Table 1.8 or the direct calculation and obtain some idea of the uncertainties inherent in this fit of such a broad range of data.

McCaslin, et al. (McC85) measured the angular distribution of yields of 670 MeV/amu Ne and Si ions stopped in a copper target. For 670 MeV/amu ^{20}Ne ions including all neutrons above 6.5 MeV at a radius of 1 meter, McCaslin found:

$$\Phi(\theta) = 372 \frac{1}{\theta} \text{ neutrons m}^{-2} \text{ per ion for } 2^\circ < \theta < 180^\circ, \theta \text{ in degrees.} \quad (1.52)$$

For incident 670 MeV/amu ^{20}Ne ions including all neutrons above 20 MeV;

$$\Phi(\theta) = 248e^{-0.26} \text{ neutrons m}^{-2} \text{ per ion for } 0^\circ < \theta < 20^\circ, \theta \text{ in degrees.} \quad (1.53)$$

and

$$\Phi(\theta) = 10e^{-0.0386} \text{ neutrons m}^{-2} \text{ per ion for } 20^\circ < \theta < 120^\circ, \theta \text{ in degrees.} \quad (1.54)$$

The neutron yields at this high specific energy for heavy ions turn out to be quite large, by integrating the above over all angles, one finds a total yield of 73.9 neutrons/incident ion for $E_n > 6.5$ MeV for ^{20}Ne incident ions. Fig. 1.29 is comparison of total neutron yields for representative heavy ions with that found for protons as a function of specific energy.

Table 1.8 Values of the parameters $\eta(Z)$ and $C(Z)$ as expressed in Eq (1.49-1.51). [Adapted from (CI83).]

Atomic Number	Element	$\eta(Z)$	$C(Z)$
1	hydrogen	1.5	1.7×10^{-4}
2	helium	2.6	3.9×10^{-6}
6	carbon	1.7	2.5×10^{-6}
8	oxygen	3.6	3.6×10^{-7}
10	neon	7.0	2.7×10^{-10}
18	argon	7.0	5.1×10^{-11}
36	krypton	7.9	6.0×10^{-12}
82	lead	11.0	1.7×10^{-13}

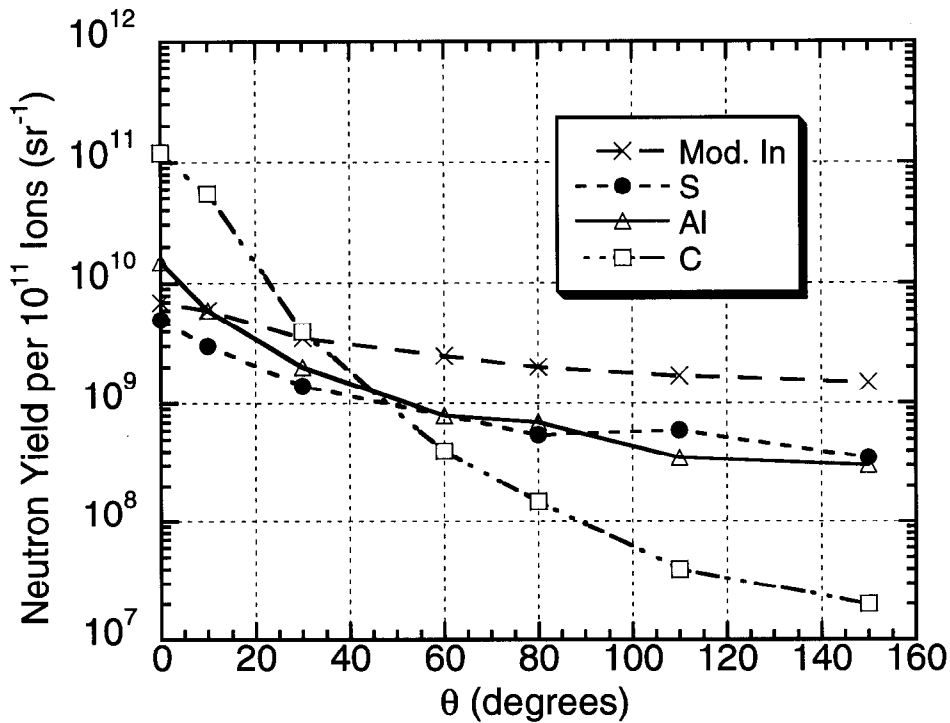


Fig. 1.27 Measured neutron yields per 10^{11} incident ions at 86 MeV/amu ^{12}C ions incident on an iron target. Activation detectors with the following sensitive regions in neutron energy, E_n , were used: moderated indium foils ($0.4 < E_n < 107$ eV), $^{33}\text{S}(n, p)^{32}\text{P}$ ($E_n > 3$ MeV), $^{27}\text{Al}(n, \alpha)^{24}\text{Na}$ ($E_n > 7$ MeV), and $^{12}\text{C}(n, 2n)^{11}\text{C}$ ($E_n > 20$ MeV). The lines are intended to guide the eye. [Adapted from (Tu84).]

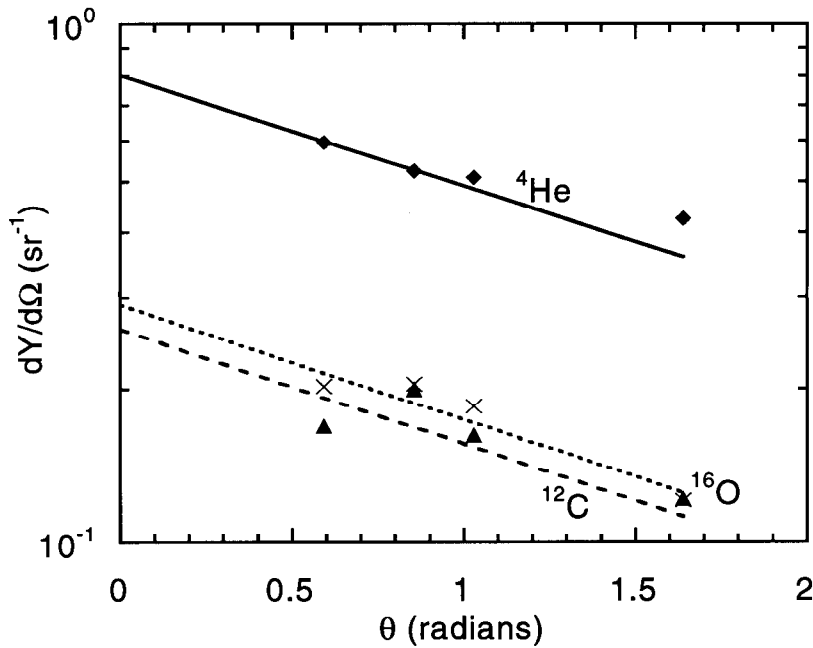


Fig. 1.28 Neutron yields per incident ion for 155 MeV/amu ions reported by Britvich, et al (Br98). The diamonds are measurements for ${}^4\text{He}$ which were fit by parameters (C {neutrons/incident ion}, β { sr^{-1} }) of (0.8, 0.49) which are defined in Eq. (1.45 and 1.46). The results for ${}^{12}\text{C}$ are denoted by triangles and were fit by (C,β) values of (0.26, 0.51). The results for ${}^{16}\text{O}$ are denoted by crosses and were fit by (C,β) values of (0.29, 0.51).

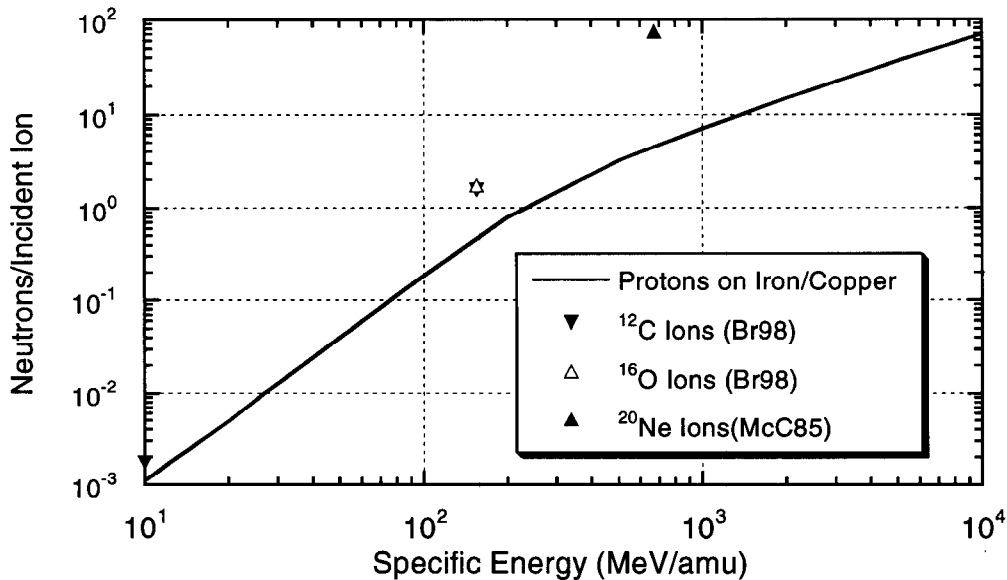


Fig. 1.29 Neutron yields as a function of specific energy for selected heavy ion projectiles as reported by the cited references. The curve for protons is that of Fig. 1.18 for protons incident on iron or copper targets. The data points for ${}^{12}\text{C}$ and ${}^{16}\text{O}$ are for a Hevimet target while the datum for ${}^{20}\text{Ne}$ is for a copper target.

Chapter 1 Composition of Accelerator Radiation Fields

References

- (Al75) R. G. Alsmiller, R. T. Santoro, and J. Barish, "Shielding calculations for a 200 MeV proton accelerator and comparisons with experimental data", *Particle Accelerators* 7 (1975) 1-7.
- (Al85) V. E. Aleinikov, A. P. Cherevatenko, F. B. Clapier, and V. I. Tsovbun, "Neutron radiation field due to 6.6 MeV/amu ^{58}Ni ions bombarding a thick Cu target", *Rad. Prot. Dos.* 11 (1985) 245-248.
- (Br98) G. I. Britvich, A. A. Chumakov, R. M. Ronningen, R. A. Blue, and L. H. Heilbronn, "Measurements of thick target neutron yields and shielding studies using beams of ^4He , ^{12}C , and ^{16}O at 155 MeV/nucleon from the K1200 cyclotron at the National Superconducting Cyclotron Laboratory, submitted to *Rev. Sci. Instrum.*, 1998.
- (Ce80) R. A. Cecil, B. D. Anderson, A. R. Baldwin, R. Madey, A. Gaolnsky, P. Miller, L. Young, and F. M. Waterman, "Neutron angular and energy distributions from 710-MeV alphas stopping in water, carbon, steel, and lead, and 640-MeV alphas stopping in lead, *Phys. Rev.* C21 (1980) 2470-2484.
- (Cl83) F. Clapier and C. S. Zaidins, "Neutron dose equivalent rates due to heavy ion beams", *Nucl. Instr. and Meth.* 217 (1983) 489-494.
- (De65) H. DeStaebler, "Similarity of shielding problems at electron and proton accelerators", Stanford Linear Accelerator Center report SLAC Pub 179 (1965). [Result also quoted in (Sc90)].
- (Gi68) W. S. Gilbert, et. al, "1966 CERN-LRL-RHEL shielding experiment at the CERN Proton Synchrotron", UCRL-17941 (1968). [Much of this material is summarized in (Pa73)]
- (Ha88) W. K. Hagan, B. L. Colborn, T. W. Armstrong, and M. Allen, "Radiation shielding calculations for a 70-250 MeV proton therapy facility", *Nuclear Science and Engineering*, 98 (1988) 272-278.
- (Hu60) E. L. Hubbard, R. M. Main, and R. V. Pyle, "Neutron production by heavy-ion bombardments", *Phys. Rev.* 118 (1960) 507-514.
- (IC73) "Data for protection against ionizing radiation from external sources", Supplement to ICRP 15, ICRP Report #21 (1973).

Chapter 1 Composition of Accelerator Radiation Fields

- (IC78) International Commission on Radiation Units and Measurements, "Basis aspects of high-Energy particle interactions and radiation dosimetry", ICRU Report No. 28, Washington, DC, 1978.
- (IC91) "1990 Recommendations of the International Commission on Radiological Protection", ICRP Report 60, (Pergamon Press, New York, 1991).
- (Ja75) J. D. Jackson, *Classical electrodynamics*, 2nd edition (John Wiley and Sons, New York, 1975).
- (Le72) G. S. Levine, D. M. Squier, G. B. Stapleton, G. R. Stevenson, K. Goebel, and J. Ranft, "The angular dependence of dose and hadron yields from targets in 8 GeV/c and 24 GeV/c extracted beams", *Particle Accelerators* **3** (1972) 91-101.
- (McC85) J. B. McCaslin, P. R. LaPlant, A. R. Smith, W. P. Swanson, and R. H. Thomas, "Neutron production by Ne and Si ions on a thick Cu target at 670 MeV/A with application to radiation protection," *IEEE Trans. on Nucl. Sci.* **NS-32**, No. 5 (1985) 3104.
- (Na78) T. Nakamura, M. Yoshida, and T. Shin, "Spectra measurements of neutrons and photons from thick targets of C, Fe, Cu, and Pb by 52 MeV protons", *Nucl. Instr. and Meth.* **151** (1978) 493-503.
- (Ne68) W. R. Nelson, "The shielding of muons around high energy electron accelerators", *Nucl. Instr. and Meth.* **66** (1968) 293.
- (Nc74) W.R. Nelson and K. R. Kase, "Muon shielding around high-energy electron accelerators, Part I, Theory, *Nucl. Instr. and Meth.*, **120** (1974) 401, and W.R. Nelson, K. R. Kase, and G. K. Svensson, "Muon shielding around high-energy electron accelerators, Part II, Experimental Investigation, *Nucl. Instr. and Meth.*, **120** (1974) 413.
- (Oh80) W. F. Ohnesorge, H. M. Butler, C. B. Fulmer, and S. W. Mosko, "Heavy ion target area fast neutron dose equivalent rates", *Health Physics* **39** (1980) 633-636.
- (Pa73) H. W. Patterson and R. H. Thomas, *Accelerator health physics*, Academic Press, New York, 1973.
- (PDG96) Particle Data Group, *Review of particle properties*, *Physical Review* **D54**, Part I (July, 1996).
- (Ra67) J. Ranft, "Improved Monte-Carlo calculation of the nucleon-meson cascade in shielding material", *Nucl. Instr. and Meth.* **48** (1967) 133-140.

Chapter 1 Composition of Accelerator Radiation Fields

- (Ra72) J. Ranft and J. T. Routti, "Hadronic cascade calculations of angular distributions of integrated secondary particle fluxes from external targets and new empirical formulae describing particle production in proton-nucleus collisions", *Part. Acc.* 4 (1972) 101-110.
- (Sc90) H. Schopper (editor), A. Fassò, K. Goebel, M. Höfert, J. Ranft, and G. Stevenson, *Landolt-Börnstein Numerical Data and Functional Relationships in Science and Technology New Series; Group I: Nuclear and Particle Physics Volume II: Shielding Against High Energy Radiation* (O. Madelung, Editor in Chief, Springer-Verlag, Berlin, Heidelberg, 1990).
- (Sh95) K. Shin, K. Miyahara, E. Tanabe, and Y. Uwamino, "Thick-target neutron yield for charged particles", *Nucl. Sci. and Eng.* 120 (1995) 40-54.
- (St83) G. R. Stevenson, "Dose and dose equivalent from muons", Rep. TIS-RP/099, CERN, Geneva Switzerland (1983). Important conclusions from this work are presented in (Sc90).
- (St85) G. R. Stevenson, P. A. Aarnio, A. Fassò, J. Ranft, J. V. Sandberg, and P. Sievers, "Comparison of measurements of angular hadron energy spectra, induced activity, and dose with FLUKA82 calculations", *Nucl. Instr. and Meth.* A245 (1985) 323-237.
- (Su89) A. H. Sullivan, "The intensity distribution of secondary particles produced in high energy proton interactions", *Rad. Prot. Dos.* 27 (1989) 189-192.
- (Su92) A. H. Sullivan, *A guide to radiation and radioactivity levels near high energy proton accelerators*, (Nuclear Technology Publishing, Ashford, Kent, TN23 1JW, England, 1992.)
- (Sw79) W. P. Swanson, "Radiological safety aspects of the operation of electron linear accelerators," Technical Report No. 188, Vienna, 1979.
- (Sw79b) W. P. Swanson, "Improved calculation of photoneutron yields released by incident electrons", *Health Phys.* 37 (1979) 347-3358.
- (Sw90) W. P. Swanson and R. H. Thomas, "Dosimetry for radiological protection at high energy particle accelerators", Chapter 1 in *The dosimetry of ionizing radiation*, Volume III (Academic Press, 1990).

Chapter 1 Composition of Accelerator Radiation Fields

- (Te85) K. Tesch, "A simple estimation of the lateral shielding for proton accelerators in the energy range from 50 to 1000 MeV," Rad. Prot. Dos. 11 (1985) 165-172.
- (Th88) R. H. Thomas and G. R. Stevenson, "Radiological safety aspects of the operation of proton accelerators", Technical Report No. 283, IAEA, Vienna, 1988.
- (Tu84) J. W. N. Tuyn, R. Deltenre, C. Lamberet, and G. Roubaud, "Some radiation aspects of heavy ion acceleration," Proc. 6th Int. Cong. International Radiation Protection Association, Berlin (1984) 673.
- (Va87) A. Van Ginneken, P. Yurista, and C. Yamaguchi, "Shielding calculations for multi-TeV hadron colliders, Fermilab Report FN-447 (1987).

Chapter 1 Composition of Accelerator Radiation Fields

Problems

- To how many GeV/s does 1 kW of beam power correspond?
 - To how many singly charged particles per second does 1 ampere of beam current correspond?
 - To how many GeV/kg of energy deposition does an absorbed dose of 1 Gy correspond?
- Which has the higher quality factor, a 10 MeV (kinetic energy) α -particle or a 1 MeV neutron? Write down the quality factors for each particle.
- Calculate the number of ^{12}C and ^{238}U atoms per cm^3 of solid material.
- Calculate the velocity and momenta of a 200 MeV electron, proton, iron ion, π^+ , and μ^+ . The 200 MeV is kinetic energy and the answers should be expressed in units of the speed of light (velocity) and MeV/c (momenta). Iron ions have an isotope-averaged mass of 52021 MeV ($A = 55.847 \times 931.5 \text{ MeV/amu}$). The π^+ mass is 140 MeV and the μ^+ mass = 106 MeV. Do the same calculation for 20 GeV protons, iron ions, and muons. It is suggested that these results be presented in tabular form. Make general comments on the velocity and momenta of the particles at the two energies. (The table may help you notice any algebraic errors that you have made.)
- Calculate the mass stopping power of a 20 MeV electron (ionization only) and a 200 MeV proton in ^{28}Si .
- An electron accelerator has a beam profile in the form of a 2 mm diameter circle uniformly illuminated by the beam. Make a crude plot of the value of the dose equivalent rate in the beam as the energy increases from 1 MeV to 10 GeV. The average beam current is 1 microamp ($1 \mu\text{A}$). Assume the beam profile is unchanged during acceleration. Compare with Swanson's simple formula ("conservative" value). Is his formula "conservative" above 100 MeV? (Hint: use Fig. 1.4.)
- Calculate the critical energy and length of material that corresponds to the radiation length for carbon and for lead. What does this say about the effectiveness of low-Z versus high-Z shielding materials for electrons?

Chapter 1 Composition of Accelerator Radiation Fields

8. A 100 MeV electron accelerator produces a $1.0 \mu\text{A}$ beam incident on a high-Z (thick) target. Estimate the bremsstrahlung absorbed dose rates at $\theta = 0^\circ$ and 90° at $r = 2$ m from the target using Swanson's rules of thumb. Compare the 0° result with the "in the beam dose equivalent rate" found in problem 6. How do the bremsstrahlung and in-beam dose rates compare?
9. Suppose the Tevatron enclosure at Fermilab is converted into an enclosure for an electron synchrotron. The radius of the synchrotron is 1000 m. If the circulated beam is 10^{12} electron, calculate the median energy of the synchrotron radiation photons for $E_0 = 100$ GeV. Also find θ_c of the "lobe."
10. For the accelerator of problem 8, calculate the neutron flux density at $r = 2$ m at large angles using the values in Table 1.3 for a high-Z (tungsten) target. Also use Table 1.3 to estimate the dose equivalent $r = 2$ m. Check this result by "guessing" the average neutron energy is 1-10 MeV and use the curve in Fig. 1.5. Compare this neutron dose with the Bremsstrahlung dose at large angles obtained in problem 8.
11. Calculate the muon fluence necessary to produce a dose equivalent of 1 mrem assuming a quality factor = 1 and that tissue is equivalent to water for minimum ionizing muons. (Hint: use Table 1.2.) Compare with the results given in Fig. 1.4 for high energies.
12. For a 20 GeV electron accelerator operating at 1 kW, the electron beam strikes a beam stop made of aluminum or iron. How long (in z) does the beam stop have to be to range out all of the muons for either aluminum or iron based on the mean range? Compare the dose equivalent rates at the immediate downstream ends of each material if 10 % of the muons leak through due to straggling and multiple scattering can be neglected. (Assume the production of muons from Fe is approximately equal to that from Al. Recall the inverse square law.)
13. One can use measurement results to check Sullivan's formula for hadron fluence above 40 MeV for high-energy proton interactions. Check the agreement for the 22 and 225 GeV/c data in Figs. 1.23 and 1.24 for 3 representative angles at one meter. (Ignore the fact that the formula is for hadrons > 40 MeV while the only data provided is for hadrons > 35 MeV and 50 MeV but do not ignore the difference between normalizing to incident versus interacting protons.) (It is valid to make the comparison on yield per interacting proton since the results in Fig. 1.24 is for targets approximately 1 interaction length long.) Comment on the quality of the agreement.

Chapter 1 Composition of Accelerator Radiation Fields

14. Calculations can also be used to check the Tesch curve for dose equivalent at $\theta = 90^\circ$ (Fig. 1.26). Use the 200 MeV calculations in Fig. 1.20 to do this by crudely numerically integrating the $60^\circ < \theta < 90^\circ$ yields to determine the average energy of the neutrons and the total fluence at $\theta = 90^\circ$ and at 1 meter. Use the results along with dose equivalent per fluence curves to obtain the dose equivalent per proton to compare with Tesch's result. (Iron is considered equivalent to copper for this problem.)
15. Use Tesch's curve in Fig. 1.26 to calculate the dose equivalent rate at 2 m and $\theta = 90^\circ$ from a target struck by $1 \mu\text{A}$ of 100 MeV protons. Compare with the neutron dose rate calculated in problem 10 for an electron accelerator having the same intensity and beam energy and discuss. (Scale the relevant result of problem 10 by the appropriate yield for copper vs. Tungsten.)
16. It is often necessary to work from fragmentary data to determine other quantities.
- a) Use McCaslin's results and the appropriate dose equivalent/fluence to calculate the dose equivalent rate at 1 meter and at $\theta = 30^\circ$ for a target struck by 10^8 ${}^{670}\text{MeV/amu}$ ${}^{20}\text{Ne}$ ions per sec. (Hint: Use all available spectrum information.)
- b) Use McCaslin's results to obtain the total yield of neutrons per ion with $E_n > 6.5$ MeV. Assuming the target to be iron or copper, how does this yield correspond to that due to 700 MeV protons? Do this for both $E_n > 6.5$ MeV and $E_n > 20$ MeV to understand the overall composition. Hint: Integrate over the unit sphere (double integral over spherical coordinates θ & ϕ)

The following indefinite integrals are needed:

$$\int \frac{\sin x dx}{x} = x - \frac{x^3}{3 \cdot 3!} + \frac{x^5}{5 \cdot 5!} - \frac{x^7}{7 \cdot 7!} + \dots$$

$$\int e^{ax} \sin bx dx = \frac{e^{ax} [a \sin bx - b \cos bx]}{a^2 + b^2}$$

The elemental area on the sphere of radius R is $dA = r^2 \sin \theta d\theta d\phi$, where ϕ is the standard azimuthal coordinate in a spherical coordinate system.

